QEX

September/October 2021

www.arrl.org

A Forum for Communications Experimenters

Issue No. 328

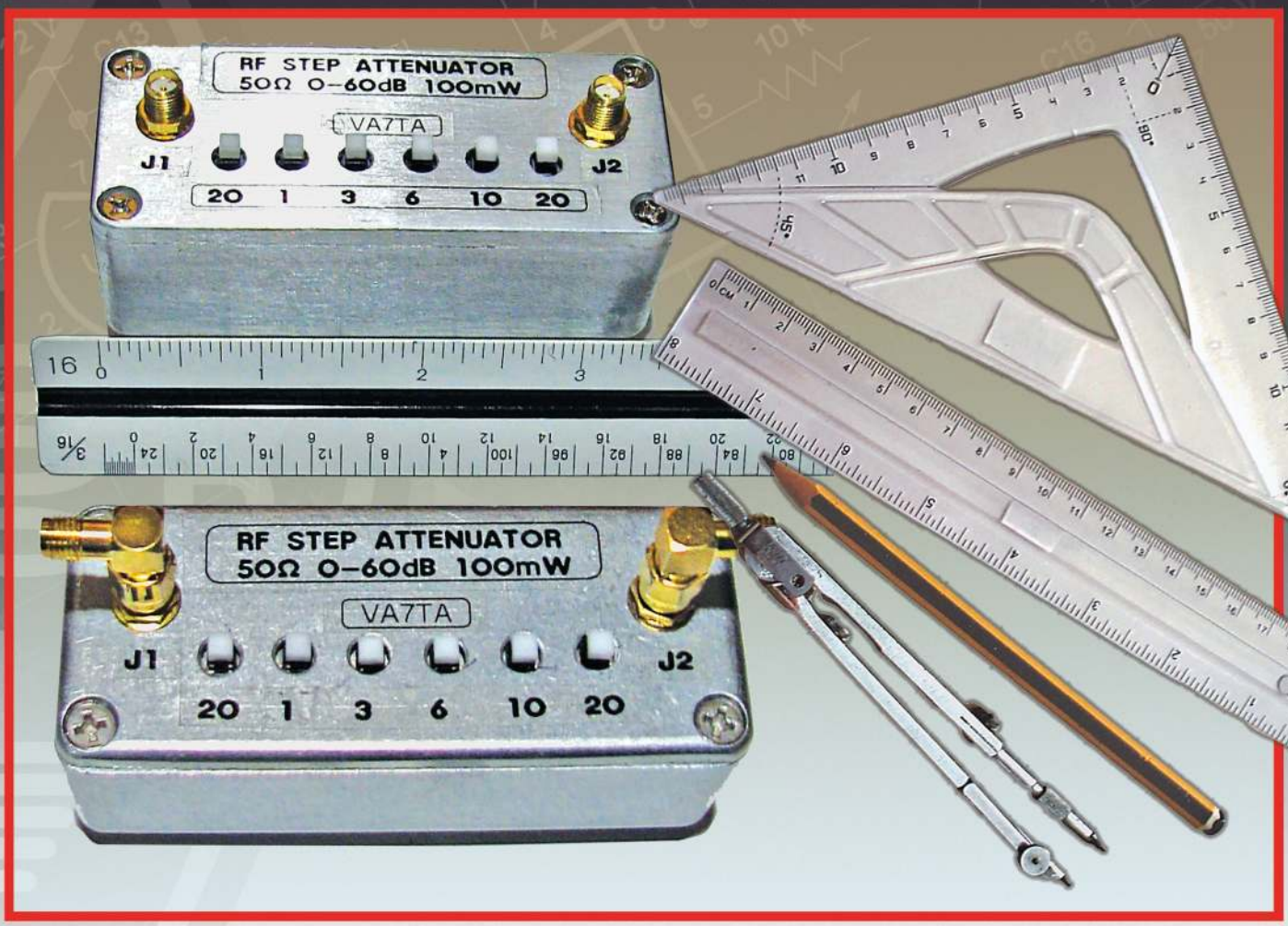

VA7TA uses integrated RF SMD components in a step attenuator design.

CT1EOJ applies drafting tools to solve a network problem.

KENWOOD

3rd IMDR 110 dB*

RMDR 122 dB*

BDR 150 dB*

Performance Exceeding Expectations.

The most happy and sublime encounters happen in the worst circumstances and under the harshest conditions.

There are enthusiasts who know this all too well because of their love of HF radio.

Results born of certainty and not circumstance. Delivered through impeccable performance. This is our offering to you.

"The Kenwood TS-890S has the highest RMDR of any radio I have ever measured."

- Rob Sherwood - NC0B - December 2018

HF/50MHz TRANSCEIVER

TS-890S

Top-class receiving performance

3 kinds of dynamic range make for top-class performance.

- Third order intermodulation Dynamic Range (3rd IMDR) 110dB*
- Reciprocal Mixing Dynamic Range (RMDR) 122dB*
- Blocking Dynamic Range (BDR) 150dB*

*Values are measured examples. (2kHz spacing:14.1 MHz, CW, BW 500 Hz, Pre Amp OFF)

- Full Down Conversion RX
- High Carrier to Noise Ratio 1st LO
- H-mode mixer

4 kinds of built-in roofing filters

500Hz / 2.7kHz / 6kHz / 15kHz (270Hz Option)

7 inch Color TFT Display

- Roofing frequency sampling band scope
- Band scope auto-scroll mode
- Multi-information display including filter scope

Clean and tough 100W output

Built-in high-speed automatic antenna tuner

32-bit floating-point DSP for RX / TX and Bandscope

Customer Support: (310) 639-4200

www.kenwood.com/usa

ISO9001 Registered

ADS#16321

QEX (ISSN: 0886-8093) is published bimonthly in January, March, May, July, September, and November by the American Radio Relay League, 225 Main St., Newington, CT 06111-1400. Periodicals postage paid at Hartford, CT and at additional mailing offices.

POSTMASTER: Send address changes to: QEX, 225 Main St., Newington, CT 06111-1400
Issue No. 328

Publisher
American Radio Relay League

Kazimierz "Kai" Siwiak, KE4PT
Editor

Lori Weinberg, KB1EIB
Assistant Editor

Scotty Cowling, WA2DFI
Ray Mack, W5IFS
Contributing Editors

Production Department

Becky R. Schoenfeld, W1BXY
Publications Manager

Michelle Bloom, WB1ENT
Production Supervisor

David Pingree, N1NAS
Senior Technical Illustrator

Brian Washing
Technical Illustrator

Advertising Information

Janet L. Rocco, W1JLR
Business Services
860-594-0203 – Direct
800-243-7768 – ARRL
860-594-4285 – Fax

Circulation Department

Cathy Stepina
QEX Circulation

Offices

225 Main St., Newington, CT 06111-1400 USA
Telephone: 860-594-0200
Fax: 860-594-0259 (24-hour direct line)
Email: **qex@arrl.org**

Subscription rate for 6 print issues:

In the US: $29

US by First Class Mail: $40;

International and Canada by Airmail: $35

ARRL members receive the digital edition of *QEX* as a member benefit.

In order to ensure prompt delivery, we ask that you periodically check the address information on your mailing label. If you find any inaccuracies, please contact the Circulation Department immediately. Thank you for your assistance.

September/October 2021

About the Cover

Tom Alldread, VA7TA, describes a low power, relatively small size step attenuator that utilizes integrated RF attenuator surface mount devices. The attenuator chips are roughly 0805 size. The low cost latching push switches used here are enclosed within a metal enclosure that eliminates the need for separate inter-stage RF shields. The components are mounted on a double-sided PCB strip that in turn is fastened to the enclosure lid via the input/output PCB edge SMA coaxial connectors.

Luiz Duarte Lopes, CT1EOJ, does not need a computer. He uses drafting tools to rigorously solve a problem that radio amateurs often face. It is the connection of a transmitter to an antenna through an impedance matching network.

In This Issue

Index of Advertisers

The American Radio Relay League

The American Radio Relay League, Inc., is a noncommercial association of radio amateurs, organized for the promotion of interest in Amateur Radio communication and experimentation, for the establishment of networks to provide communications in the event of disasters or other emergencies, for the advancement of the radio art and of the public welfare, for the representation of the radio amateur in legislative matters, and for the maintenance of fraternalism and a high standard of conduct.

ARRL is an incorporated association without capital stock chartered under the laws of the state of Connecticut, and is an exempt organization under Section 501(c)(3) of the Internal Revenue Code of 1986. Its affairs are governed by a Board of Directors, whose voting members are elected every three years by the general membership. The officers are elected or appointed by the Directors. The League is noncommercial, and no one who could gain financially from the shaping of its affairs is eligible for membership on its Board.

"Of, by, and for the radio amateur," ARRL numbers within its ranks the vast majority of active amateurs in the nation and has a proud history of achievement as the standard-bearer in amateur affairs.

A *bona fide* interest in Amateur Radio is the only essential qualification of membership; an Amateur Radio license is not a prerequisite, although full voting membership is granted only to licensed amateurs in the US.

Membership inquiries and general correspondence should be addressed to the administrative headquarters:

ARRL
225 Main St.
Newington, CT 06111 USA
Telephone: 860-594-0200
FAX: 860-594-0259 (24-hour direct line)

Officers

President: Rick Roderick, K5UR
P.O. Box 1463, Little Rock, AR 72203

The purpose of *QEX* is to:

1) provide a medium for the exchange of ideas and information among Amateur Radio experimenters,

2) document advanced technical work in the Amateur Radio field, and

3) support efforts to advance the state of the Amateur Radio art.

All correspondence concerning *QEX* should be addressed to the American Radio Relay League, 225 Main St., Newington, CT 06111 USA. Envelopes containing manuscripts and letters for publication in *QEX* should be marked Editor, *QEX*.

Both theoretical and practical technical articles are welcomed. Manuscripts should be submitted in word-processor format, if possible. We can redraw any figures as long as their content is clear. Photos should be glossy, color or black-and-white prints of at least the size they are to appear in *QEX* or high-resolution digital images (300 dots per inch or higher at the printed size). Further information for authors can be found on the Web at **www.arrl.org/qex/** or by e-mail to **qex@arrl.org**.

Any opinions expressed in *QEX* are those of the authors, not necessarily those of the Editor or the League. While we strive to ensure all material is technically correct, authors are expected to defend their own assertions. Products mentioned are included for your information only; no endorsement is implied. Readers are cautioned to verify the availability of products before sending money to vendors.

Kazimierz "Kai" Siwiak, KE4PT

Perspectives

Progress in Technology

On a hot July day in the southwestern USA desert a mother ship launched a manned rocket plane that flew higher than 50 miles – the "edge of space." The year was 1962 when Robert M. White flew to a height of 59.6 miles in an X-15 rocket powered aircraft. The mother ship, a USAF B-52 aircraft, launched twelve flights that exceeded an altitude of 50-miles. This includes two missions that exceeded the 62-mile (100 km) high Kármán boundary between Earth's atmosphere and outer space. In July of 2021 the 50-mile altitude mark was breached by a commercial Virgin Galactic passenger-carrying rocket-powered aircraft launched from a purpose-built mother ship. This was followed on July 20 — the 52nd anniversary of the first manned Moon landing — by a passenger-carrying Blue Origin sub-orbital rocket flight, à la NASA's Alan B. Shepard flight, which exceeded the Kármán altitude boundary.

It took just six decades of technological progress to go from the X-15 rocket plane research project, and from NASA's first sub-orbital manned rocket flight, to the onset of space tourism by two different methods. *QEX* salutes and congratulates the technologists and visionaries involved.

In This Issue

- Tom Alldread, VA7TA, designs a small RF step attenuator that is accurate over a wide frequency range.
- Luiz Duarte Lopes, CT1EOJ, graphically solves a matching network using drafting implements.
- Eric Nichols, KL7AJ, in his Essay Series, organizes the use of Kirchhoff's laws.
- Steve Stearns, K6OIK, explains a paradox where the additional transmission line loss due to SWR can be negative in dB.
- Lynn Hansen, KU7Q, describes the CTR2 HMI for managing radios in your shack.
- Maynard Wright, W6PAP, shows that SWR can depend on amplifier output impedance.

Writing for *QEX*

Please continue to send in full-length *QEX* articles, or share a **Technical Note** of several hundred words in length plus a figure or two. *QEX* is edited by Kazimierz "Kai" Siwiak, KE4PT, (**ksiwiak@arrl.org**) and is published bimonthly. *QEX* is a forum for the free exchange of ideas among communications experimenters. All members can access digital editions of all four ARRL magazines: *QST*, *On the Air*, *QEX*, and *NCJ* as a member benefit. The *QEX printed edition* is available at an annual subscription rate (6 issues per year) for members and non-members, see **www.arrl.org/qex**.

Would you like to write for *QEX*? We pay $50 per published page for full articles and *QEX* Technical Notes. Get more information and an Author Guide at **www.arrl.org/qex-author-guide**. If you prefer postal mail, send a business-size self-addressed, stamped (US postage) envelope to: *QEX* Author Guide, c/o Maty Weinberg, ARRL, 225 Main St., Newington, CT 06111.

Very kindest regards,
Kazimierz "Kai" Siwiak, KE4PT
QEX Editor

Tom Alldread, VA7TA

7056 Railway Ave., Courtenay, BC, Canada V9J 1N4; **va7ta@rac.ca**

Miniature SMA RF Step Attenuator

This design utilizes integrated RF attenuator surface mount device components that are very accurate over a wide frequency range.

An RF step attenuator that provides a user friendly means for varying RF transmission path loss is a useful accessory for numerous amateur radio applications. Some examples are: to vary the output level of a signal source in calibrated steps, extend the measurement range of a signal analyzer, prevent the overload of a broadband receiver module, or as a comparison reference to establish the loss of a network. This step attenuator, which uses miniature SMA type coaxial connectors and wide band RF attenuator surface mount components, makes a convenient palm size companion for a number of small SDR receiver dongles. It also could prove to be a useful accessory for some of the portable, inexpensive RF measurement instruments that have recently become available such as the nanoVNA1 [1] and the tinySA [2].

Some traditional relatively large size step attenuator designs utilize toggle switches that required inter-stage shielding to prevent stray coupling. They typically were based on attenuator stages made up from multiple resistor combinations, some lacked wideband accuracy and because of the need for inter-stage shielding, they were relatively complex to build.

This article describes how to build an inexpensive, low power, relatively small size step attenuator similar to those shown in **Figure 1**. These attenuators have a 60 dB range and are small enough to fit in the palm of one's hand. They have demonstrated excellent accuracy to mid VHF frequencies and, with less accuracy, are still usable to 450 MHz.

Figure 1 — SMA RF step attenuators with accessories.

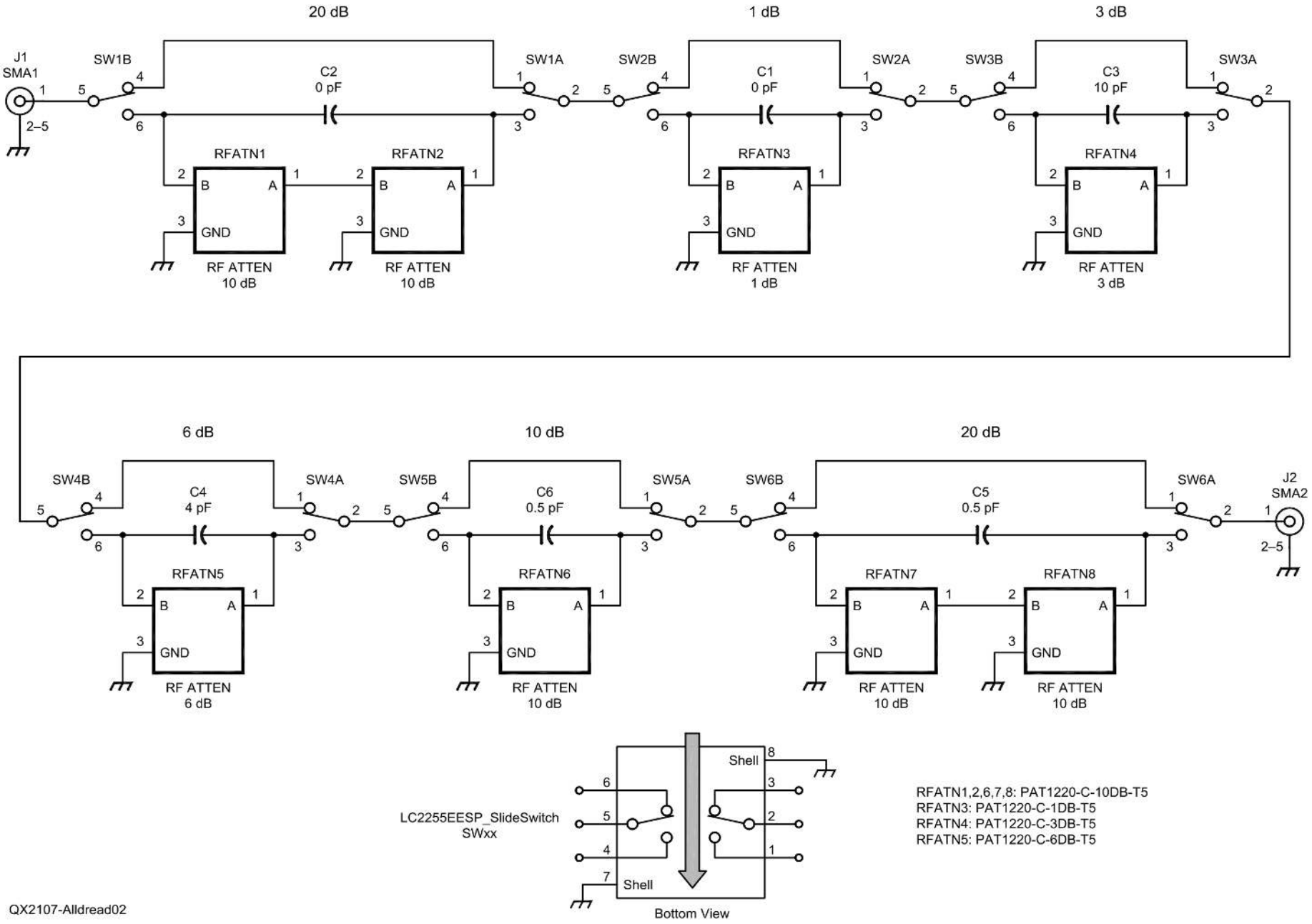

Figure 2 — SMA step attenuator schematic. The parts are listed in Table 3.

This design utilizes integrated RF attenuator surface mount device (SMD) components that are rated for microwave use up to 10 GHz. They are available in 1 dB increments up to 10 dB, and cost about 50 cents each. Since only one chip is needed for most attenuation stages they provide a very inexpensive, tidy, highly accurate wideband solution for this application. The attenuator chips are roughly 0805 size, which most builders find are large enough to install using regular soldering tools while using commonly available magnification such as that provided by a magnification light or hood. The low cost latching push switches used here are enclosed within a metal body that eliminates the need for the provision of separate inter-stage RF shields. The components are mounted on a double-sided PCB strip that in turn is fastened to the enclosure lid via the input/output PCB edge SMA coaxial connectors. This PCB mounting method eliminates the need for any additional mounting hardware. Chassis work is easy, since the die-cast aluminum enclosure is fully prepared by simply drilling holes in the front panel lid according to the drilling template pattern provided here. This should be an easy single weekend project for the experienced builder.

Circuit Description

As shown in the **Figure 2** schematic, this attenuator has 6 stages that occupy the full length of the small Hammond 1590A type, die cast aluminum enclosure. The design has some flexibility since the step sizes can easily be changed to suit one's needs by simply installing different loss attenuator chips. The chips are available with losses in 1 dB increments from 0 to 10 dB. The first attenuator that I built has a maximum attenuation of 50 dB and a pair of 10 dB steps. The second version, described here and shown in **Figure 2**, has two 20 dB steps and a maximum attenuation of 60 dB. The additional 10 dB range is provided by replacing the second 10 dB step with a 20 dB step, which I deemed preferable after measuring the enclosure stray coupling. I found it to be much higher than 60 dB, which confirmed that it was feasible to incorporate an additional 10 dB of range. This was determined by doing a frequency sweep with the 1 dB attenuator chip removed and with all attenuator stages switched in.

I provided step sizes of 20, 1, 3, 6, 10, 20 dB. A 2 dB step was not provided due to space limitations. The 2 dB increment was not considered as important as optionally using the last available stage to provide a higher maximum loss setting. The 1, 3 and 6 dB steps were considered significant for inclusion. The 1 dB step is important for calibration checks. The 3 and 6 dB steps are important for measuring the half-power and half-voltage points of a signal and have significance for checking response bandwidths and S-units.

The two SMA connector ports connect directly to the 20 dB stages, see **Figure 2**. These stages consist of two 10 dB attenuator chips in cascade. The SW1 – SW6 DPDT switches either bypass or insert the attenuator chip stages into the transmission path depending on the desired selection. The direct connection of the 20 dB attenuation stages to the SMA connectors at each end of the circuit maximizes the stray path isolation of the attenuator. This is important when using high attenuation settings. When both 20 dB stages are inserted into the signal path the most extreme high and low level signals within the attenuator enclosure travel only on very short PCB traces at each end of the PC board. This helps minimize the stray coupling between the input and output ports.

Mounting pads for compensation capacitors, that can be used to provide improved UHF response by compensating for stray high frequency losses, are provided for each stage. However not all stages are equipped with capacitors, note C1 and C2 are 0 pF in **Figure 2**. The values shown were selected empirically based on through-path swept frequency response and good port SWR across the spectrum of interest.

RF Performance Measurements

The swept frequency response loss from each individual stage and also the steps in cascade were measured with the wide dynamic range Signal Hound SA44B

Figure 3 — Signal Hound loss and nanoVNA SWR frequency sweep.

Table 1 – SMA step attenuator setting and measured attenuation for various frequencies.

Attenuator setting, dB	*3 MHz*	*30 MHz*	*50 MHz*	*150 MHz*	*222 MHz*	*300 MHz*	*440 MHz*
0	0.06	0.11	0.14	0.29	0.31	0.54	0.57
1	0.95	1.00	1.03	1.20	1.24	1.47	1.50
3	3.07	3.11	3.17	3.32	3.44	3.63	3.81
6	6.05	6.10	6.11	6.27	6.37	6.51	6.72
10	10.05	10.08	10.08	10.26	10.36	10.57	10.75
20	19.99	20.06	20.07	20.16	20.20	20.41	20.37
30	30.14	30.13	30.03	30.28	30.28	30.53	30.80
40	40.13	40.06	39.97	40.22	40.29	40.58	40.84
50	50.08	50.01	49.91	50.26	50.50	51.09	51.76
60	60.03	59.83	59.88	60.80	61.51	62.80	65.10

spectrum analyzer and companion tracking generator pair shown in **Figure 3**. The step attenuators shown here were the earlier versions. The frequency response resulting from one of the measurements with the attenuator set to 30 dB is shown in **Figure 4**. Direct views of some of the screen captured tracking generator measurement results can be downloaded from the ARRL **QEXfiles** web page **[3]**. The magnified vertical scale in **Figure 4** provides a detailed view of the response from 3 to 450 MHz where the high end rolls off about 0.8 dB.

Table 1 shows the measured insertion losses obtained from similar frequency sweeps for 10 of the possible step attenuator settings. Results for steps from 0 to 60 dB at 7 frequencies from 3 to 440 MHz are listed. All steps up to 50 MHz were within 0.33 dB. Steps from 0 to 50 dB were within 0.50 dB up to 222 MHz. For 440 MHz the losses remain within 1 dB of the setting up to 40 dB. Note that for many cases the step change values are very close, which is an important consideration when making relative measurements. For example at 150 MHz the difference between the 30 and 40 dB steps is (40.22 – 30.28) = 9.94 dB, off by just 0.06 dB. For UHF signals the high insertion loss 50 and 60 dB steps are still of use for trouble shooting despite the diminished accuracy.

The quality of impedance match in terms of SWR for all the stages was measured using the nanoVNA (also seen in **Figure 3**). **Figure 5** shows SWR graphical results for the 6 dB setting obtained via the PC *nanoVNASaver* software application. **Table 2** lists SWR measurements at the marker frequencies obtained from similar tests for each of the steps. The quality of impedance match agreed very nicely with SWR results for all attenuation stages up to 150 MHz at better than 1.1:1 and better than 1.25:1 at 450 MHz.

For a practical test I made a comparison

Table 2 – Measured SWR for SMA step attenuator settings at various frequencies.

Attenuator setting, dB	*3 MHz*	*30 MHz*	*50 MHz*	*150 MHz*	*450 MHz*
0	1.01	1.02	1.02	1.06	1.17
1	1.01	1.01	1.01	1.02	1.25
3	1.00	1.01	1.01	1.02	1.10
6	1.00	1.00	1.01	1.03	1.20
10	1.01	1.01	1.01	1.02	1.25
20	1.01	1.02	1.03	1.07	1.21

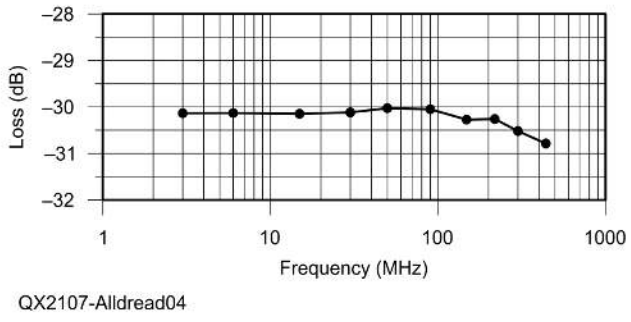

Figure 4 — 30 dB step frequency response from 3 to 450 MHz.

to my HP 8656B high quality signal generator. I set my HP8656B to 14.2 MHz in CW mode at a level of –100 dBm for starters. I connected it via the SMA step attenuator to an SDRplay RSP1 **[4]** type receiver controlled by spectrum analyzer software. I set the spectrum analyzer *y* – axis to 2 dB/div. I set the span to a narrow 1 kHz, an 8 Hz resolution bandwidth, and with 100 measurement averaging. With the step attenuator set to 0 dB I found the measured level to be –100.6 dBm. The HP8656B level was then increased to –70 dBm and the attenuator set to 30 dB using three different attenuator stage combinations. The measurement results were:

J1_20 + 10 dB = –100.6 dBm

J2_20 + 10 dB = –100.5 dBm

J2_20 + 6 + 3 + 1 dB = –100.5 dBm.

In all three cases in the middle of the HF band the step attenuator matched the HP8656B attenuator to within 0.1 dB. It was amazing to see how closely the SDR receiver spectrum analyzer measurement matched the absolute output level of the signal generator. Of interest for verifying the possibility of using the TinySA generator output as a signal source for receiver sensitivity testing, it was likewise set to –70 dBm at 14.2 MHz and used as the signal source in place of the HP8656B. The measured level was –101.1 dBm roughly a half a dB lower than the HP8656B output level, very close indeed!

The Switch Solution

My previous experiences with more than one commercial step attenuator have not always been that great because of erratic switch contact performance. In some cases toggle switches were used that did not have gold plated contacts that presumably had become tarnished or corroded [5]. The switches were essentially sealed and as such not designed to permit cleaning with contact cleaner. Nothing much could be done for repairing the problem except replacing the switches, which wasn't very practical to do.

The mechanical design of the plunger-activated slide switches chosen for this design is a nice fit for this application, since the switch metal body doubles as the inter-stage shield and the contact slider design presents a low impedance to the RF path. I would have preferred switches with gold plated contacts, however I could not find any with similar mechanical design features nor any that were affordable.

Initially I built two attenuators using very inexpensive switches that I purchased online from a source in China. I based the mechanical design and the PCB artwork layout for the use of these very economical switches. To make a long story short, I found the contact resistances to be unstable and higher than spec. Cleaning the contacts with a good contact cleaner got them to work okay for a while but after being left unused for a month or two the problems resurfaced.

In pursuit of a better switch alternative I tried a somewhat more expensive set of switches from a North American supplier. Fortunately they have a matching mechanical design and have an identical PCB footprint that matched my existing PCB board artwork. Based on the spec sheet illustrations these alternative switches looked almost identical to ones I initially used, thus I got the impression that they may have been made by the same manufacturer. I wasn't optimistic that they would be any better. But upon delivery and close examination I noticed these alternative switches were clearly a more rugged design. I built up two more attenuators using these slightly pricier switches. I was delighted to discover the contact resistances measured lower than spec and remained consistent. There was no need to mess with any contact cleaning. The extra cost for a full set of the better switches amounts to about US$6 total per attenuator, which is less than half the cost of a can of contact cleaner; clearly it is a better choice. At the time of this writing the alternative switches recommended here continue to work flawlessly.

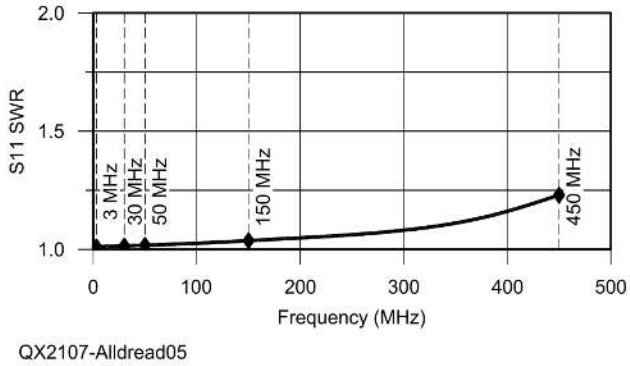

Figure 5 — 6 dB step SWR frequency sweep from 50 kHz to 450 MHz.

Parts Acquisition Tips

The parts cost per attenuator can be reduced significantly if a small group gets together to build several attenuators, and purchase a small batch online of bare PC boards, enclosures and connectors from a supplier in Asia. In a quantity of 5 or 10, printed circuit boards can be delivered by courier to North America from a variety of PCB houses in China for $5 or less per board. The enclosure

Table 3 – Parts list.

Reference	*Description*		*Manufacturer Part #*	*Manufacturer*	*Digi-Key #*
RFATN1,2,6,7,8	RF ATTENUATOR 10DB 50OHM 0805	5	PAT1220-C-10DB-T5	Susumu	PAT1210CT-ND
RFATN3	RF ATTENUATOR 1DB 50OHM 0805	1	PAT1220-C-1DB-T5	Susumu	PAT121CT-ND
RFATN4	RF ATTENUATOR 3DB 50OHM 0805	1	PAT1220-C-3DB-T5	Susumu	PAT123CT-ND
RFATN5	RF ATTENUATOR 6DB 50OHM 0805	1	PAT1220-C-6DB-T5	Susumu	PAT126CT-ND
C5,6	CAP CER 0.5PF 50V C0G/NPO 0805	2		Yageo	311-1094-1-ND
C4	CAP CER 4PF 50V C0G/ NPO 0805	1		Yageo	311-1093-1-ND
C3	CAP CER 10PF 50V C0G/NPO 0805	1	CC0805JRNPO9BN100	Yageo	311-1099-1-ND
SW1,2,3,4,5,6	SWITCH PUSH DPDT 0.3A 30V	6	LC2255EESP	E-Switch	EG5891-ND
J1,2	CONN SMA JACK STR 50OHM EDGE MNT	2	732512120	Molex	WM5536-ND
RF tight Enclosure	BOX ALUM UNPAINTED 3.64"LX1.52"W	1	1590A	Hammond Manufacturing	HM150-ND
rubber feet	BUMPER HEMI .37" DIA X .21" BLK	1	BS22BL05X06RP	Bumper Specialties Inc.	2042-1050-ND
Bare PC Board	Order direct from Mfr or contact VA7TA	1	Gerber Step Atten zip file	JLCPCB	N/A

and connectors can also be purchased online from Asian sources at a lower cost compared to North American pricing. However the purchasing of the enclosure and connectors from Chinese sources may not be worth the inconvenience for making just a single attenuator considering the typical tardy delivery times for low-cost shipping methods and minimal saving for a one-off build. The SMD chips and better quality switches need to be purchased from local suppliers — fortunately they are quite inexpensive.

Table 3 includes a reference parts list intended as a guideline for the identification and procurement of components.

Construction

Figure 6 shows the switch side of the completed PCB, which is mounted via the SMA connectors to the underside of the enclosure lid. The pads for the compensation capacitors can be seen behind the switch housings. **Figure 7** is a view of the attenuator chip side of the PCB. The two pairs of cascaded 10 dB attenuators that make up the 20 dB stages can be seen at each end of the PCB. The manufacturing Gerber files for the PCB are contained within a zip archive that is available for download from the ARRL **QEXfiles** web page **[3]**. The author has a few extra boards left over from the batch which was obtained from a professional PCB manufacturer that are available to those that may wish to purchase just a single board via regular letter mail delivery.

To ensure proper switch plunger shaft alignment with the front panel holes, the two SMA PCB edge coaxial connectors should be left unsoldered to the PCB until after mounting to the enclosure lid. This allows for the shifting of the PCB ever-so-slightly for final switch plunger actuator shaft alignment to the front panel hole centers. Once proper alignment has been achieved the connectors can be soldered to fix the PC board in place. I found with one connector I needed to bend one of the connector ground tabs out slightly to match up with the corresponding PCB pad.

Figure 6 — Step attenuator PC board, switch body side up view.

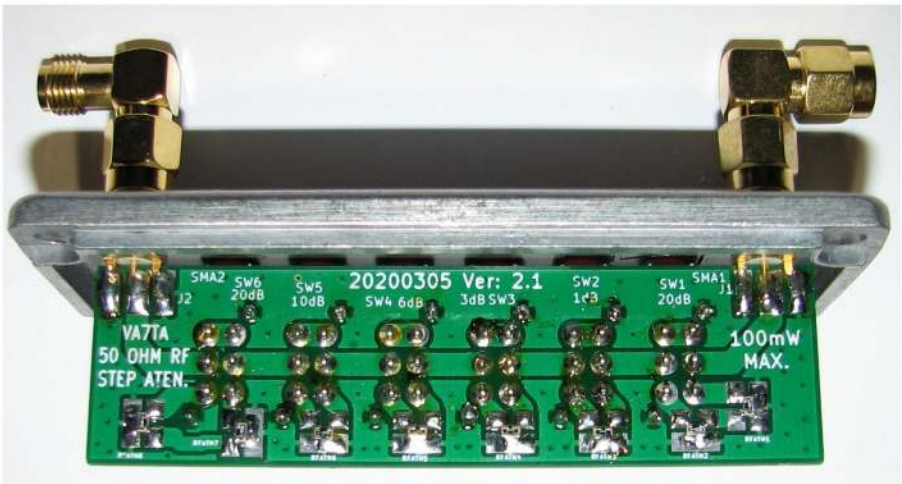

Figure 7 — Step attenuator PC board , attenuator SMD side up view.

Figure 8 is a close up view of the plunger shaft style slide switch. I attached 1/4" cylindrical caps for my very first attenuator (see **Figure 3**). A downside to using caps is that they require larger holes in the front panel, which could lead to signal leakage. I discovered that the plunger shafts are long enough to protrude beyond the front panel and the switches can be easily operated without caps. I decided to not use caps for later versions. I found it easier to tell the attenuation IN/OUT position of the switches without the plunger shaft caps. A black indicator band that is visible only when the shaft is out (i.e., when the attenuator stage is bypassed) can be drawn around the plunger shaft with a very fine marking pen.

A drilling template graphics file is also available for download from the ARRL **QEXfiles** web page **[3]**. **QEXfiles: Photo7** shows the drilling template that I used for the first attenuator version. It is shown centered and taped to the enclosure lid front panel face. The template has since been updated mainly to specify smaller holes for the switch plunger shafts without caps. It is important to use a template to achieve proper positioning of the holes. The template graphics file has 100 mm scale calibration lines for each dimension. After printing, it is important that the line lengths on the printed copy be carefully measured and confirmed to be within the 99.5 to 100.5 mm range. Once the template is cut out, properly positioned and securely taped to the panel face, a center punch was used to accurately mark the holes. Then a small diameter, 1/16" bit was used to drill pilot holes through each punch mark. Then progressively larger bits were used to enlarge the holes to the final size as specified on the template. For the recommended design without the push button knob caps 13/64" holes are used for the switch plunger shafts and 1/4" holes for the SMA connectors. To ensure the square switch shafts don't catch on the sharp edges of the 13/64" holes a larger 5/16" bit should

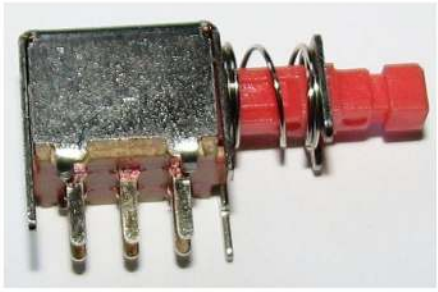

Figure 8 — Plunger style slide switch.

be spun by hand from both the inside and outside of the front panel to bevel-shave the sharp edges off each switch shaft hole.

To confirm the switches are functional, the through resistance of all the switch contacts in cascade should be measured with a low measurement voltage digital ohm meter set to the lowest scale. This is done by setting the attenuator to 0 dB, which bypasses all of the attenuation stages. A pair of extra SMA female PCB connectors was used with short SMA jumper cables to connect to the attenuator. Alligator test leads completed a secure connection to the ohm meter. With the attenuator set to zero the center conductor through resistance should measure no more than a few tenths of an ohm. The attenuator described here measured 0.1 Ω. The actual meter reading was 0.7 Ω as the test lead resistance was found to be 0.6 Ω leaving 0.1 Ω within the attenuator. Exercising each switch from **BYPASS** to **INSERT** and back to **BYPASS** did not change the all-bypassed reading. In contrast, after not being used for a few months my first attenuator with the switches purchased from an Asia supplier measured 4.0 Ω, after exercising the switches the resistance dropped to 1.9 Ω, dramatic consistency difference between switches! To put this into perspective, an unwanted 5 Ω switch contact resistance within this 50 Ω transmission impedance environment would result in roughly a 10% voltage drop, which would be roughly equivalent to 1 dB additional unwanted insertion loss.

High humidity and moisture from condensation is the contact corrosion enemy. As shown in **QEXfiles: Photo 8,** to maintain a dry environment, a couple of small packets of silica gel desiccant were placed in the bottom of the housing prior to closing the enclosure. I plan to replace the gel packs about once a year, which I think should keep the switches nice and dry.

QEXfiles: Photo 9 shows the completed attenuator labeled with Brother Ptouch® self adhesive label tape. Rubber stick-on feet were attached to the bottom of the enclosure, which helps prevent the attenuator from sliding around and of course protects bench/desktop surfaces.

Applications

The RF step attenuator compared to other attenuator types offers spur-of-the-moment ease of use for the operator. In comparison fixed coaxial attenuator alternatives, which must be swapped out to change the path loss, are relatively awkward to use. In the case of the SMA type coaxial attenuator this swapping involves the process of loosening and re-torquing the connector retaining nuts. In applications where the attenuation value needs to be changed rapidly, fixed attenuators are not practical. In such applications the step attenuator shines.

This project could provide a good accessory for many RF signal sources with fixed level outputs. It could be used to provide an adjustable output level capability for a number of inexpensive RF generator module designs that can be purchased online. Most are based on either direct digital synthesizers that are best operated at full output level or PLL integrated circuits that have fixed output levels.

The step attenuator can be a useful accessory for extending the output level range of signal sources for making measurements. As mentioned above, the recent tinySA2 **[2]** handheld battery operated spectrum analyzer has a signal generator feature. Its output level can be varied from –6 to –76 dBm. However the –76 dBm output, which is close to S9 on an S-meter, is too high a level for receiver sensitivity testing. This attenuator could be used as a tinySA accessory to provide levels as low as –136 dBm (0.0355 μV) to accommodate measuring typical receiver sensitivity.

Limitations

The maximum power rating of the attenuator chips is 100 mW, which is less than traditional step attenuators that use half watt resistors. However the power handling range could be extended to a full 2 W with the use of an external 20 dB SMA barrel attenuator accessory (**QEXfiles: Photo 10**). These SMA attenuators are available in several different loss values from an online supplier **[6]**. The right angle SMA adapters (**QEXFiles: Photo 10**) are a convenience that allow the use of shorter and/or less flexible test leads when the attenuator is used on a bench top.

Conclusion

This attenuator design provides very accurate insertion loss steps for RF signals up to mid VHF frequencies and remains usable with some accuracy limitations up to the 70 cm amateur band. It can be built using low cost readily available components and is easy to build with hobbyist level electronics construction tools. With minimal routine maintenance it should provide many years of reliable service.

*Tom Alldread, VA7TA, was interested in electronics since grade school. In his teens he repaired radio and television sets. He obtained his amateur radio license in 1965, and upon graduating from technical college obtained his commercial radio operator certification. He graduated from the Capitol Radio Engineering Institute Engineering Technology program. Tom worked in the telecommunications industry as a microwave, multiplex and VHF radio equipment maintenance technician, an instructor, an engineering standards and design specialist, and in the Middle East as adviser for long distance network operations management. Now retired, Tom and his wife Sylvia, VA7SA, live on Vancouver Island. Tom, is a member of The Radio Amateurs of Canada, enjoys operating CW, designing equipment, and supporting emergency communications. He has been net manager for the SSB/CW 20 meter Trans-Canada Net (**www.transcanadanet.com**) for more than a decade. His interests include microcontroller development projects associated with amateur radio. Tom won second place in the Luminary 2006 DesignStellaris contest and first place in the 2011 Renesas RX contest. Other hobbies include computing, RVing, hobby farming and bicycling.*

Notes:

[1] **https://groups.io/g/nanovna-users/**.
[2] **https://groups.io/g/tinysa/**.
[3] **www.arrl.org/qexfiles**.
[4] **https://www.sdrplay.com/spectrum-analyser**.
[5] **https://www.finishing.com/**.
[6] **https://www.aliexpress.com/**.
Additional resources listed here are on the **www.arrl.org/qexfiles** page:
QEXfiles Photo 7 – Drilling template taped to enclosure front panel lid.
QEXfiles Photo8 – Desiccant pack humidity protection.
QEXfiles Photo9 – Assembled step attenuator completed with labels.
QEXfiles Photo10 – Recommended accessories: right angle adapters and 2 W 20 dB attenuator.

Lynn H. Hansen, KU7Q

10914 Westchester Dr., P.O. Box 301, Lava Hot Springs, ID 83246; **lynn@lynovation.com**

CTR2 – An HMI for All of Your Radios

The CTR2 Human-Machine-Interface is intended as a fixed station accessory providing control and audio management for the large variety of radios and components in your shack.

To be useful, machines usually have ways for humans to interact with them. From a simple ON/OFF switch to controlling a machine using a modern touch panel controller, the purpose of machine control is to allow interaction with humans. Machine control systems are commonly referred to as Human Machine Interfaces (HMIs). So it is in amateur radio. Every radio on the market has an HMI of sorts. For years, the radio front panel with its dials and switches served as its HMI. The latest radios feature touch screen controls with virtual dials and buttons replacing dials and switches. Spectrum displays are the norm rather than an expensive accessory.

Ever since the first PC hit the market, hams have been creating new HMIs in software for their radios. Even if you don't own the latest radio, your PC can give your old radio modern features. But what if you're like me with radios of various vintages scattered around your shack? Or maybe you've invested heavily into high-end keys, microphones and headsets, and primarily use one radio because it's such a hassle to disconnect and reconnect these accessories? What about the new digital modes? Wouldn't it be nice to use any radio in your shack using a single PC USB cable?

Figure 1 — The basic multi-radio CTR2 system consists of the HMI board, an RJ45 adapter board, a color remote display, a manual RJ45 switch, and a couple of radio I/O modules.

Some History

In 2001 I created a Pocket PC program I called Control The Radio (CTR). Along with that software, I designed a Bluetooth® serial interface named BlueLync that allowed you to control your radio wirelessly. CTR and BlueLync were published in the February 2007 issue of *QST*. The software could control of any number of BlueLync equipped radios by simply connecting to the radio of interest. After using CTR for a while I was struck by just how useful a common user interface was for all of my radios. Unfortunately, the Pocket PC, CTR, and BlueLync became dinosaurs after the iPhone® came out later that year.

I really liked the convenience of a common user interface with its shared frequency list. I thought about updating CTR

and BlueLync to work with the newer cell phone technologies but decided against it. By then there were already many radio control and logging programs available for these devices. While wireless connectivity is a neat party trick I ultimately decided that Bluetooth added an unnecessary layer of complexity. I wanted something modern, simple to expand, that took advantage of the latest technologies, managed audio — which the original CTR did not do — provided digital signal processing, had all the normal options like keyers and decoders, and wasn't integrated into a cell phone, tablet, or PC. I also wanted to use it on all of my radios from my 35 year old TS-680 to my new FTDX101.

The Radio Multiplexer

Over the years the thought of a common user interface still resonated with me so I set out to create a full-featured standalone HMI that could interface with all of my radios — a radio multiplexer if you will. Advancements in microprocessor technology offer interface and control options that I only dreamt of 20 years ago. I call my HMI *Control The Radio Too* (CTR2) because controlling the radio is just one of many functions it performs. It's a self-contained radio HMI that manages up to 16 different radios and allows me to use a single key, microphone, headphone, and computer (if needed) with all of my radios. Each radio looks the same as far as controlling its basic features (frequency, mode, Tx and Rx audio). **Figure 1** shows the basic multi-radio CTR2 system consisting of the HMI board, an RJ45 adapter board, a color remote display, a manual RJ45 switch, and a couple of radio I/O modules. **Figure 2** shows a functional drawing of this system.

CTR2 uses a modular design approach. You build only what you need now. Additional features can be added later as your needs expand. Option boards stack on top of the HMI board and interconnections are done using 10-wire ribbon cables. There are currently four option boards:

1) An RJ45 adapter board. This board adapts the 10-pin ribbon cable to an RJ45 jack so a manual RJ45 switch can connect to the HMI as seen in **Figure 1**.

2) A four-to-sixteen port RJ45 switch that automatically routes the radio I/O (audio, serial CAT control, PTT, and key) from the selected radio to the HMI.

3) A radio antenna switch controller that controls one or two 8-port commercial antenna switches (such as the DX Engineering RR8B-HP) to automatically route a common antenna to the selected radio.

4) An antenna switch controller that controls an 8-port commercial antenna switch, which automatically selects one or multiple antennas (for phased arrays) and routes them to the common antenna port. A different antenna can be selected for each band. A fully configured CTR2 system is shown in **Figure A** on the **www.arrl.org/QEXfiles** web page.

The CTR2 HMI

The CTR2 HMI is totally self-contained and does not require an external computer to operate. At its core is a Teensy 4.1 development board from **PJRC.com [1]**. This board contains a 600 MHz ARM Cortex-M7 processor, 1 GB RAM, 2 GB of Flash memory, a micro-USB interface, an SD memory slot, and host of serial ports and other interfaces. An optional ESP8266 can be installed in the HMI to support Wi-Fi connectivity. Wired Ethernet is also available via an expansion kit, but I have not yet exploited that feature.

Audio is managed by the Teensy Audio Adapter **[2]**. This little marvel includes the NXP SGTL5000 codec that converts audio to and from digital. Once in digital form the chip provides mixers, amplifiers, oscillators, and signal routing via virtual patch cords. **PJRC.com** provides the Arduino libraries to support the SGTL500 chip but they've gone one better. They provide an audio design tool **[3]** that allows you to easily configure the SGTL5000 functions without writing a single line of code. **Figure B** on the **QEXFiles** web page is a screenshot of the CTR2 audio interface as designed on the PJRC audio design tool. If you're interested in interfacing audio to microprocessors, you should check out the PJRC web site. Paul Stoffregen at **PJRC.com** and his online community have done an amazing job creating a microcontroller/audio ecosystem that just about anyone can use.

A Nextion enhanced serial display **[4]** connects to the HMI via CAT5 cable. This allows the display to be placed in the most convenient location on your operating style.

Two programs run concurrently to create the HMI. The main program runs on the

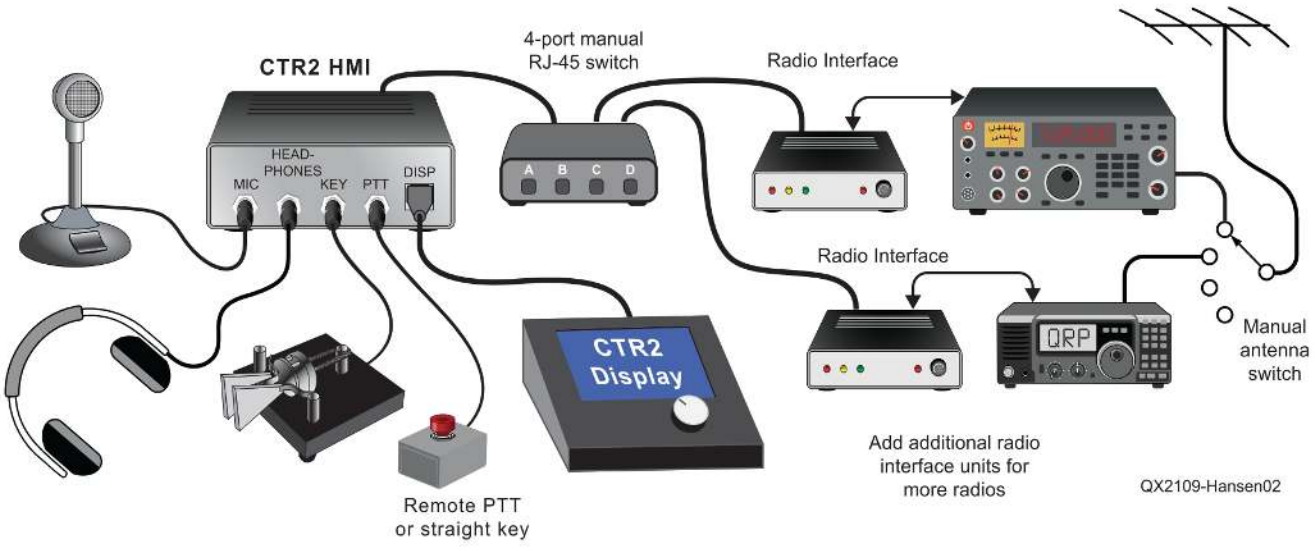

Figure 2 — A functional drawing of the basic CTR2 system.

Figure 3 — The Home page is where most of the radio interaction occurs.

Figure 4 — Screen shot of the Radio Select page.

Teensy processor. This program is written in Arduino code using the Teensyduino add-on available at **PJRC.com** and is open source. It handles the time sensitive tasks such as Morse encoding and decoding, file management, etc. The second program runs on the Nextion display and was created using the Nextion Editor **[4]**. It uses a unique C-like coding environment and is extremely powerful. The display program handles the user interface including page rendering and touch control. The two programs communicate continuously across the serial link to stay in sync with each other. Source code for both programs is available on the **QEXFiles** web and will be hosted on GitHub in the future.

The user interface is page-based and operates like a browser. The *Home* page (**Figure 3**) is where most of the radio interaction occurs. Pressing the [Back] button of the other pages returns you to the *Home* page.

The top line in **Figure 3** controls the transmit buffer system in CW and RTTY modes. Pressing the [Keyboard] button in the top left opens a virtual keyboard that can be used to compose messages that are transmitted when the [Enter] key is pressed. Touching the [Menu] button next to the [Keyboard] button opens the *Tx Buffer* page where you can select, edit, or delete the ten messages for each mode (including voice mode). Touch [Select] in the *Tx Buffer* page then touch a message to transmit it. In addition, there are ten buttons across the top of the *Home* page that instantly transmit that buffer when pressed. Once a message starts transmitting you can pause and restart it, or touch the [X] button to delete it. The Rx buffer is on the second line. This is where decoded CW or RTTY text is displayed. Touch the Rx message area to display the full 512 character buffer.

The third line starts with the [Radio Select] button (R2:A4 in the photo). R2:A4 means Radio 2 and Antenna 4 are selected and a red background indicates the radio is using the shared database. **Figure 4** is a screen shot of the **Radio Select** page. Each radio port can be named. Red text indicates that port is using the shared database. Back on the *Home* page the name of the radio is displayed at left-center, below the date and time. The rest of the third line contains the log buttons. The [Auto>] button parses the Rx buffer to find anything that looks like a call sign or RST report. Simply touch the desired data to add it to the log entry.

The audio spectrum display and gain controls are immediately below the third line. The spectrum displays the upper or lower sideband from 100 to 3200 Hz. In CW and RTTY modes, tuning cursors are displayed to assist in tuning the decoders. Filter cursors are also displayed here if either the low-pass or notch filters have been moved into the audio passband. The notch filter follows tuning changes so it remains on the interfering carrier. Touching a signal on the FFT display retunes the radio to place that signal approximately in the decoder's range. Selecting the low-pass or notch filter on the encoder, then touching the display places the selected filter at that location.

The [<] and [>] buttons on either side of the FFT display allow you to step through the 100 memory channels. The sliders on the right adjust the FFT gain, volume, and audio squelch level. More about the squelch control later.

The three buttons at left-center allow you to select the operating band (and radio model), radio mode, and operating mode. The frequency is displayed in the center. You can adjust frequency by clicking the top or bottom of any digit, rotating the encoder (changes by the selected step – the digit shown in red), or pressing the [Keypad] direct entry button on the next line down. Of course you can also turn the radio dial too! The [Lock] and [A/b] VFO, and [>0] at right-center allow you to lock the display, toggle A/B VFOs, and set all digits to the right of the selected digit to 0.

The second to last line contain VFO/Memory functions. The [V<P] sends the previous frequency and mode to the VFO. This is handy when you tune off frequency or switch radios and want to return to the frequency and mode you had selected previously. The [V>M] (VFO to Memory) button allows you to save the current frequency and mode to the favorites list. The [Keypad] button opens the frequency input page. The [V<M] button allows you to select a

Figure 5 — Screen shot of the favorites list page.

frequency from memory and mode from your favorites list. **Figure 5** shows a screen shot of the favorites list page.

The [Scan] button allows you to specify the scan type, frequency or memory. In frequency scan you can define the range, step, and speed. In memory scan you can choose the start and end memory location.

The options menu is on the bottom line. The bottom right button is the Transmit Enable. When set to [Tx Off] you can use the paddle to practice code. In **Figure 3** [Iambic-B] indicates the paddle mode selected and that Transmit is enabled. Pressing the key will send the code to the transmitter and turn this button red. The [Settings] button takes you to the setting page for the selected mode. You can also edit the settings of other modes while in this page. [Log] displays a summary of your log. Touching the [Freq] button cycles through the functions of the rotary encoder. As each function is selected its associated control on the display is highlighted in red. Turn the encoder to change the selected control's settings. Finally, [Help] opens a help page that contains useful program information, common Q-signals, and the phonetic alphabet.

What Else Does It Do?

The CTR2 HMI also includes the following.

• It can be powered from any voltage source from 9 to 36 V dc as designed. 18 to 72 V dc can be used if the 18 to 72 V dc/dc converter is installed. It needs at least 300 mA at 12 V. Polarity is normally negative ground but cutting JP2 allows positive grounded or floating battery systems to be used.

• It supports Icom, Kenwood, and most Yaesu radio protocols. It also supports the Icom PCR-1000 receiver and the Flex 6000 series radios. It only controls frequency and mode so most implementations of these protocols by other manufacturers work as well. Options like S-meters, power control, etc., vary widely among radios so I chose not to support them.

• The rotary encoder normally tunes the frequency by the selected frequency step. Pressing it steps through various options that can also be adjusted. In voice, RTTY, and digital modes the encoder allows you to change the Tx audio level during transmit by simply turning the encoder. This is handy in digital modes like FT8 where power levels change as you move around the pass band. In CW transmit mode, turning the encoder during transmit changes the keyer speed — a very handy feature.

• Touching the spectrum display moves the selected signal to the tune decoder cursor and automatically shifts the tune frequency step to 10 Hz for fine tuning CW and RTTY signals with the encoder.

• A USB-A host port supports a USB keyboard and mouse. The keyboard works with the CW and RTTY keyers and the mouse emulates the rotary encoder for tuning and option selection. A virtual keyboard is included so a physical keyboard is not required.

• Each radio port has its own settings unique to that radio. There is also a common database of favorite frequencies, band stacking registers, antenna configurations, and transmit buffers that all radios can share. Settings can be copied to other radio ports.

• Basic standalone logging is supported, including contest sequence numbering and exchange text. The log is saved in ADIF format on the SD card and can be downloaded via the built-in web server.

• The HMI can create a Wi-Fi access point or connect to your local Wi-Fi network. This feature is not fully developed yet but a simple web server is functional. A Wi-Fi network is required to control a Flex radio.

• CW mode supports straight key, pass-through, Iambic-A and B, Ultimatic, and Bug modes. Pass-through allows you to use the selected radio's keyer instead of the built-in keyer in CTR2. Ten transmit CW buffers are available per radio port plus ten more in the shared database. CW mode has its own adjustable low-pass and notch filters and receive audio is emphasized around the selected side tone frequency.

• In voice mode 5-band equalizers are available for Tx and Rx audio. Voice mode has its own adjustable Tx level, low-pass and notch filters. A ten buffer voice keyer is also included. Message length is limited only by the size of the SD card. The shared database includes ten more voice buffers.

• RTTY mode supports, 45.45, 50, 75, and 100 baud with 170, 225, 425, 450, and 850 Hz carrier shifts. Ten transmit RTTY buffers are available per radio port with ten more in the shared database. RTTY mode has its own adjustable Tx level, low pass and notch filters and receive audio is enhanced around the higher carrier frequencies.

• A computer is required for digital modes such as PSK31 and WSJT-X. In digital mode the HMI emulates a USB sound card and provides a USB serial interface. Configure your digital program to use the Teensy USB audio interface for Tx and Rx then set the Tx level. For third-party applications the HMI appears as a Kenwood TS2000 radio on the USB serial port. Your program controls the frequency and mode of the HMI using the Kenwood protocol. The HMI in turn will control whatever radio is selected on the radio interface side using that radio's control protocol. The HMI also allows you to monitor transmit and receive audio on the USB port, which is nice when you just want to listen to what's going on.

• Off-air recording is supported in all modes. Receive recordings are limited to the size of your SD card. The maximum SD card size is 32 gigabytes.

• When the optional antenna control board is installed, the HMI can automatically select a different antenna (or antennas in the case of phased arrays) for each band.

• In Beacon mode the HMI displays the currently active beacon from the International Beacon project **[5]** on the selected band. The internal real-time clock should be calibrated with WWV for this to work properly. Beacon frequencies are pre-programmed in memory slots 91 to 95.

• A WWV decode option allows the internal clock to automatically synchronize with the IRIG time codes broadcast by WWV/WWVH **[6]**. WWV frequencies are pre-programmed in memory slots 96 to 100. Due to fading and distortion, synchronization may take some time.

• CTR2 provides a VOX circuit with an adjustable threshold. This is great for voice, RTTY, and digital modes since no additional keying circuit is required for your radio. You can also set VOX to just pass Tx audio to your radio and use your radio's VOX circuit or an external PTT if you desire. ***CAUTION:*** *Windows may switch USB audio ports on its own. If it switches the microphone input to the Teensy board and HMI's VOX is active, audio from your PC will be transmitted over the air. You should disable transmit mode on the HMI when not using it.*

• Finally, CTR2 has an adjustable all mode audio squelch that allows you to mute Rx audio until the band gets busy. This helps alleviate the fatigue that sets in when listening to band noise all the time. This is similar to using squelch on FM but it works when the audio level increases.

Design Considerations

Circuit schematics and bill of materials for all boards are posted on the **QEXfiles** web page. While the design is quite straight-

forward, there are a few interesting features to note. First, I use CAT5 cable to connect the radio interfaces to the HMI. This allows use of readily available, inexpensive cables. However, this created two problems.

First, operators can get confused with what plugs into what. The HMI *does not* use an Ethernet interface to the radio I/O modules or the display. Never plug a CAT5 cable from the HMI into an Ethernet device. Wires 7 and 8 on the HMI interconnection are used for +5 V dc and ground. Therefore, if you use Power over Ethernet (PoE) devices and plug an HMI cable into your network you could run into trouble. *I suggest clearly labeling CTR2 cables to minimize this possibility.* Also note that the RJ45 jack for the remote display is on the front of the HMI, next to the 3.5 mm audio and keying jacks. Radio I/O RJ45 jacks exit the rear of the HMI.

Second, I wanted balanced audio (i.e. transformer isolation) between the radios and the HMI for noise immunity. To squeeze Line-In and Line-Out audio (4 wires), +5 V dc and ground (2 wires), transmit and receive serial (CAT) data (2 wires), PTT and Key signals (2 wires) into 8 wires I used a trick I learned years ago in the telecom industry. Using CT (center tapped) transformers on each end of the audio paths provides two extra wires because the normal audio paths are balanced through the transformers (i.e. have no ground reference). The CT of the transformer makes the audio pair look like a single wire. The two signals, audio and dc control, are independent of each other. **Figure 6** is a simplified diagram of how this is done.

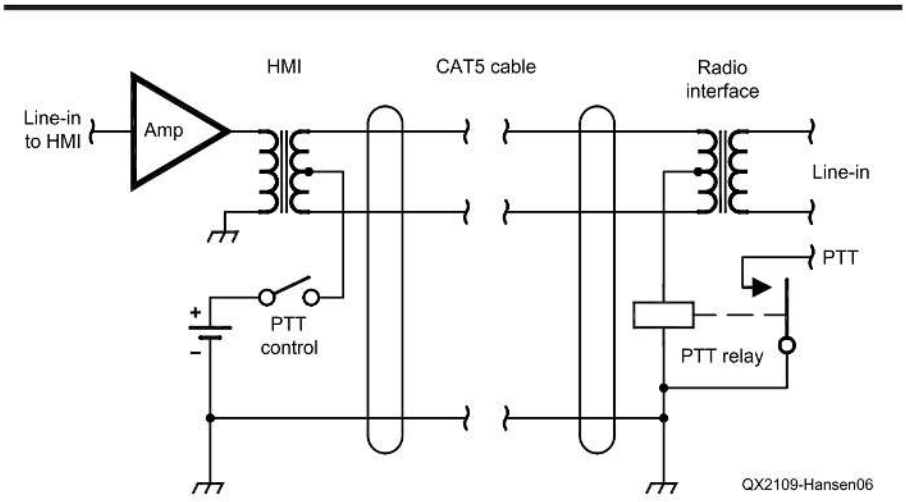

Figure 6 — Simplified interconnection diagram.

Radio I/O Modules

CAT serial port level conversion is done in the radio I/O module. This makes the HMI radio port agnostic to the electrical interface of the radio it's connected to. Early in the digital age the 'big three' radio manufacturers each developed their own unique serial interfaces. Over time, it's just become a headache for the owners. There are three standards. Icom has the CI-V interface, which is a two-wire bus scheme that allows multiple radios to share the same connection on a single pair of wires. Kenwood has their IF-10C interface that provides a non-inverted three-wire TTL interface, which interfaced to yet another add-on (IF-232C) to provide RS232 levels. The radio I/O module can interface directly to the IF-10C. Yaesu used a three-wire non-inverted TTL method similar to the Kenwood IF-10C. In time, most manufacturers just installed RS-232 ports on their radios. The design of the CTR2 radio I/O module accommodates all three methods through a switch matrix similar to what I used on CTR-BlueLync. Even though it is 5 V based, it will work on RS-232 lines using the inverted settings, as long as your RS-232 line receiver doesn't expect the voltage to go below zero volts.

ULN2803A Darlington transistor arrays are used as line drivers for all control signals on the radio interconnect cabling. This provides isolation for the microprocessor's I/O pins and allows signal inversion when needed in the level converter. They also drive the LEDs built into the RJ45 jacks. On the HMI end, the RJ45 LEDs indicate Tx and Rx data to and from the radio on the control port. Both flashing is a good sign. On the radio interface end, the RJ45's LEDs indicate PTT and Key output status (LED is ON when active).

Reed relays drive the PTT and Key output lines to the radio. The relays can switch up to 200 V at 0.5 A, any polarity. There is a 1 ms delay on the relay close and open operations. Jumpers can be installed to bypass the relays and use the output of the ULN2803A instead. It can switch up to 50 V dc, 0.5 A, positive polarity only. There is no delay in the ULN2803A output.

I used high-frequency bypass capacitors and ferrite beads liberally to eliminate RFI problems. If you experience RFI you may need to add additional ferrite chokes to all the interface lines.

Let's Build It

This project uses surface mount devices (SMDs) so the only viable construction method is with pre-populated PCBs. You can build a temporary system on a breadboard if you want to try it out or experiment with it. **Figure 7** shows the project in the early stages of development. Bread-boarding is a good way to prove a concept, but you'll find that audio and digital signals don't play nicely together on flying wires. In this configuration, simply moving a wire affects the received noise floor.

Perf-board construction is not recommended even if you use through-hole components because most of the connectors are not perf-board friendly.

I can supply PCBs with the SMD components already installed. All that's needed is to add the connectors and header pin jacks. Because board prices drop drastically in quantity, I'll queue orders until I can order 50 at a time. My web page will have ordering information. **Figure 8** shows a close-up of the HMI and the RJ45 port adapter PCBs.

Automated Bill of Material (BoM) files for the boards are available for download from the **QEXfiles** web page. These files run in your browser and make it easy to order the parts or build each board. **Figure C on QEXFiles** shows the front of the HMI board in the automated BoM. Click the [B] button to switch to the back side. There are columns to track sourcing parts and placing them. As you move the mouse cursor over each part on the list, the corresponding parts on the board are highlighted showing their location. You can also click on a device on the board and it will be highlighted on the part list.

On the HMI, install jumper JP3 on the

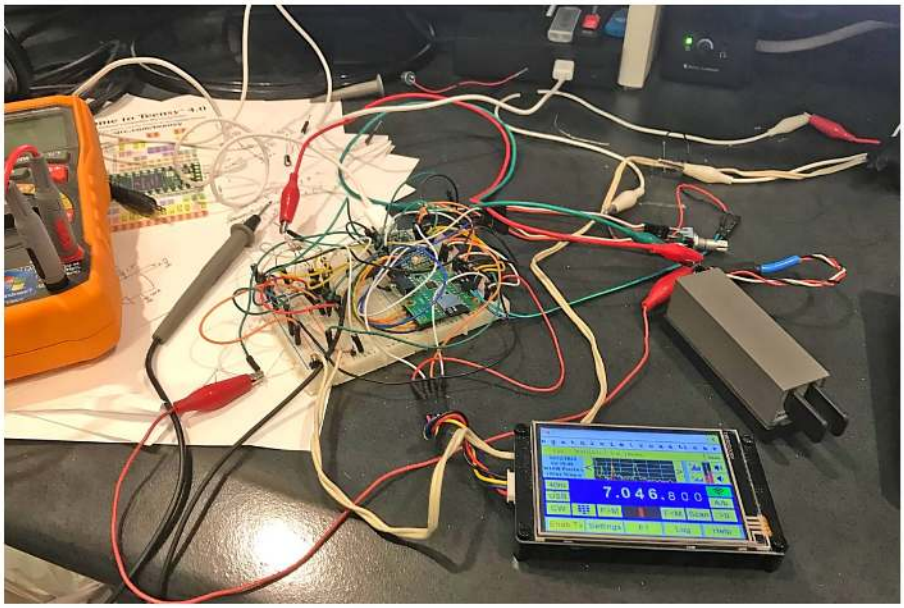

Figure 7 — The project in the early stages of development.

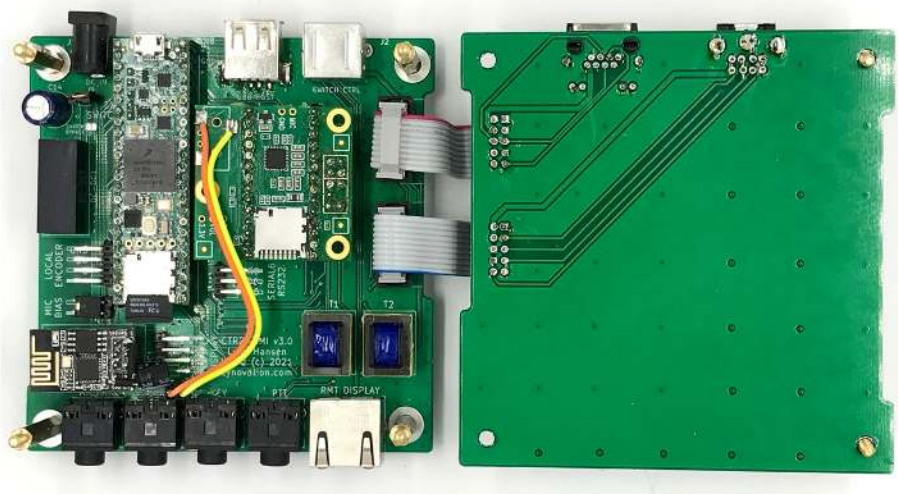

Figure 8 — A close-up of the HMI and the RJ45 port adapter boards.

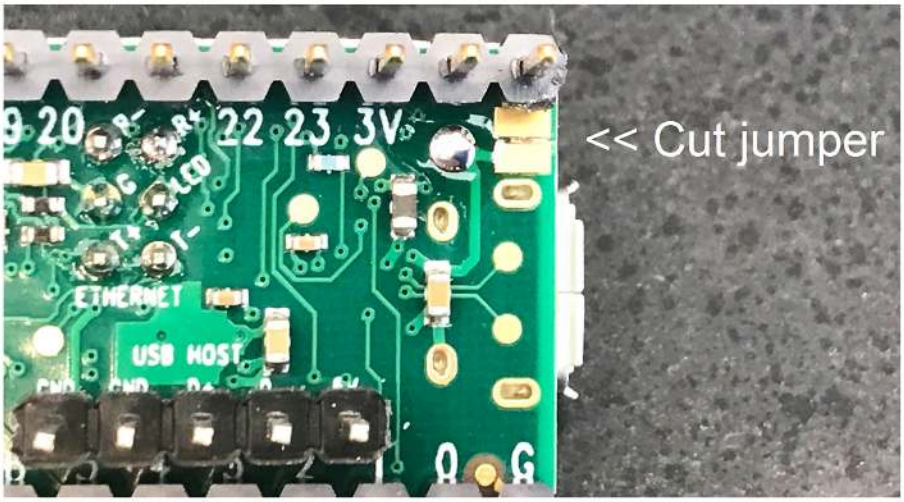

Figure 9 — Isolate the Teensy from USB power by cutting the indicated jumper.

Mic Bias header if you are using an electret microphone. Header pins J9 allow you to connect an external switch on the HMI. Solder across jumper JP1 to bypass the external switch.

You must build the RJ45 adapter board to use the HMI with a manual RJ45 switch. This board is not required if you install the automatic RJ45 switch option.

The display driver board just requires the RJ45 connector and pin headers to be installed. On the radio I/O module, leave JP1 open and install RV1 if you want an adjustable attenuator on Line-In. Insert a jumper on JP2 and install R4 (8 to 32 Ω, 2 W) to add a speaker termination resistor if you will be using the speaker jack on the radio for Line-In. Don't install the relays, and solder across JP3 and JP4 if you want to use solid-state keying. Header J1 allows you to select +5 V dc or ground on pin 8 of the terminal block. The +5 V dc source is current limited to about 40 mA by 120 Ω resistor R8.

A 12-pin pluggable terminal strip is used for the radio interface. This provides a universal interface but you'll need to build custom cables to fit the radios you are using. The Line-In and Line-Out lines are transformer isolated and dc blocked.

A Word about Power

CTR2 is intended to be a fixed station accessory providing control and audio management for the large variety of radios in your shack. It has a large input voltage range of 9 to 36 V and requires up to 500 mA at 12 V dc. It can even run on –24 V dc or –48 V dc if you cut JP2 to isolate the power input negative lead from ground. If –48 V dc operation is desired, replace the EC4SAW-24S05N dc-dc converter with an EC4SAW-48S05N, increase the voltage ratings of C16, C17, and C18 to 75 V dc, and cut JP2.

Nominally the system pulls around 240 mA on a 12 V supply (450 mA on the +5 V dc side of the converter). This can briefly spike to over 800 mA on the 5 V side when the ESP8266 Wi-Fi module is transmitting. While it is tempting to power the Teensy from the USB connection to your PC, the PC USB port is not able to supply the current required to power all of HMI options such the Wi-Fi, the 5-inch display, and the optional CTR2 switches. It is also not advisable to have the USB 5 V power connected when the Teensy is being powered externally. To isolate the Teensy from USB power turn the Teensy 4.1 board over and cut the jumper (**Figure 9**) between the pads next to the +5 V pin.

Packaging It

The CTR2 system was designed so that additional option boards such as the automated RJ45 switch and antenna controller boards stack on top of the HMI using 25 mm standoffs. This forms a self-supporting framework that doesn't require an enclosure. The display enclosure is a simple wedge shape cut from acrylic.

CNC files are available for the cube and display enclosures. They were created in the Shapeoko Carbide Create program **[7]**. Even if you don't have access to a CNC mill, these files will give you the dimensions needed to cut the cases.

I can supply a limited number of pre-cut display enclosures.

The radio I/O module is mounted in a PacTec 115129 CN-XRL housing (**Figure 10**). One end is cut to fit the RJ45 jack and the other end exposes the 12-pin pluggable terminal connector used to wire the radio interface. **Figure 11** shows a close-up of the radio I/O terminal block wiring. A #14 AWG copper wire is folded back and connected to two ground pins to form a strain relief.

Figure 10 — The radio I/O module is mounted in a PacTec 115129 CN-XRL housing.

Firmware

The firmware for this project is open source and is licensed for non-commercial use only. Contact me if you have any questions regarding this licensing. Understanding the code might be a little daunting at first since there are two separate systems interchanging information with each other. I've tried to document the functions in the code in my own style. Yours will undoubtedly be different than mine. Reviewing the code will give you an idea of what it takes to create a device like the HMI.

Source code files are available from he **QEXfiles** web page. I will eventually place these on GitHub repositories. There are three sets of source code files, one for the Nextion 3.5-inch display, one for the Nextion 5-inch display, and one for the Teensy 4.1 board.

The source files can be modified in any text editor. All options are free for individual developers and are available for Windows, Mac, and Linux (except Visual Studio). You must install the Arduino IDE to download the binary file to the Teensy board.

The Nextion display firmware requires the Nextion Editor to modify and compile programs for the displays. This is a free Windows program **[8]**, which provides drag and drop visual editing of the HMI screens. The binary file (.tft) from this program is then copied to an SD card that is then inserted into the SD card slot on the display. At power-up the display detects this file and updates the onboard firmware. This is an easy option for customizing any of the displays to your liking.

The project's firmware is not mature and not necessarily bug-free. This is a learning experience for me. It works as intended but there is a lot of room for improvement. Some of the features are experimental and not fully debugged. A forum user's tag line says it all; "Hardware eventually fails. Software eventually works." I plan to continue pushing my limits and welcome suggestions and help from others.

Final Comments

Future plans include developing the Wi-Fi and Ethernet interfaces. This would allow the HMI to be controlled remotely from anywhere. My desire was to design and build a custom expandable radio HMI. I now have a test bed to experiment with new ideas.

Much of my inspiration comes from the pages of *QST* and *QEX* magazines. The inspiration for this project came from an article by Rick Dubbs, WW9JD, in the April 2020 issue of *QST*. Rick described the keyer he designed using the Nextion display.

I would like to thank my son, Matt, KE7AQM, for his help and perseverance in converting me to KiCad 3D modeling and

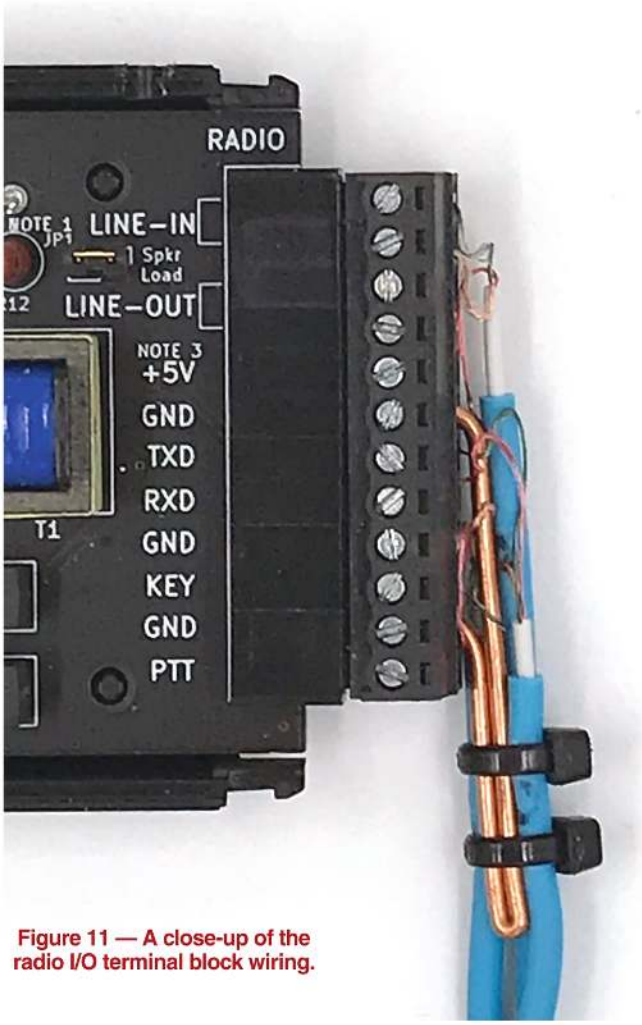

Figure 11 — A close-up of the radio I/O terminal block wiring.

the automated BOM.

I plan on offering board sets and I can cut a limited number of display and HMI enclosures on my CNC if there's enough interest. A user's manual and additional information can be found on my web page **[9]**.

ARRL member Lynn Hansen, KU7Q, was first licensed in 1971 as WN7QYG at age 14. Within a year he upgraded to WA7QYG, then achieved the Amateur Extra class license in 1981 while studying for his Commercial Class Radio Telephone license. His amateur radio experience and several Cleveland Institute of Electronics home-study courses enabled him to follow a life-long passion of working in electronics and communications as a communications technician, an engineering assistant, and finally as an operations manager over a large multi-state utility communications network. Now retired, he has the time to follow his passions, such as this project.

References

[1] **https://www.pjrc.com/store/teensy41.html**.

[2] **https://www.pjrc.com/store/teensy3_audio.html**.

[3] **https://www.pjrc.com/teensy/gui/**.

[4] **https://nextion.tech/enhanced-series-introduction/**.

[5] **https://www.ncdxf.org/beacon/**.

[6] **https://www.nist.gov/pml/time-and-frequency-division/radio-stations/wwv/wwv-and-wwvh-digital-time-code-and-broadcast**.

[7] Free download at; **https://carbide3d.com/carbidecreate/**.

[8] **https://nextion.tech/nextion-editor/**.

[9] **www.lynovation.com/**.

Letters

Analysis, Design and Verification of SA602A IC Hartley Oscillators, (May/June 2021)

Dear Editor,

John E. Post, KA5GSQ, shows a very interesting use of the *Spice* program for an *LC* oscillator at about 1 MHz. I will address some circuit improvements that are based on analysis in *Ansoft Harmonica*. I opted to take the RF power from the collector, which is not atypical. The phase noise and output power can both improve significantly. Referring to Post Figure 2 with component values of Figure 3, I reduced the emitter resistor R_E from 20,000 Ω to 2,000 Ω, reduced the coupling capacitors C_{bypass} to the tuned circuit from 1 µF down to 5 pF, and interchanged the inductor values of *L* and *nL* so that the smaller inductance is on the bottom. This reduces the loading on the base of transistor *Q*2, which according to my *Ansoft Harmonica* simulation not only gets the output power up by more than 10 dB, but improves the phase noise by more than 20 dB. Thus, an 800 kHz oscillator phase noise is −140 dBc/Hz at 1 kHz offset, and an 80 MHz oscillator phase noise is −130 dBc/Hz at 10 kHz offset. This kind of analysis can not be done in *Spice* — *Best regards, Ulrich L. Rohde, N1UL*; **dr.ulrich.l.rohde@gmail.com**.

From the Editor,

Thank you for your observation that different analysis programs can lead to different optimization opportunities for oscillator circuits. — *73, QEX Editor.*

Send your *QEX* Letter to the Editor, via email to qex@arrl.org. We reserve the right to edit your letter for clarity, and to fit in the available page space. *QEX* Letters may also appear in other ARRL media. The publishers of *QEX* assume no responsibilities for statements made by correspondents.

Steve Stearns, K6OIK
P.O. Box 4917, Mountain View, CA 94040-0917; **steve.stearns@comcast.net**

Loss Formulas for General Uniform Transmission Lines and Paradox 5

Transmission lines with complex characteristic impedance make possible a paradox where the additional loss due to SWR can be negative in dB.

Loss formulas are presented and discussed for general transmission lines whose characteristic impedance can be complex. The 1997 loss formula of W7XC is proved. Examples illustrate the error in calculated loss when characteristic impedance is assumed to be real but isn't. A surprising "paradox" shows that the additional loss due to SWR can be sub-unity (negative in dB). This phenomenon is studied. It is found that deliberate mismatching can be advantageous if done correctly but not by conjugate matching.

Introduction

The author's article "General Uniform Transmission Lines," *QEX*, May/June, 2020, generated considerable interest **[1]**. The article prompted correspondence concerning loss formulas. The present article is a response to that apparent interest and may be considered an addendum or a sequel. The original article presented and explained *four paradoxes* involving transmission lines:

- Reflection coefficient magnitude greater than unity
- Negative SWR
- Sub-unity return loss
- Time prediction by anti-matching.

Here the focus is specifically on loss formulas for a transmission line whose characteristic impedance is complex. Several examples are given to illustrate the error in calculated loss when characteristic impedance is assumed to be real, but isn't. Complex characteristic impedance makes possible *a fifth paradox*:

- The additional loss due to SWR can be negative in dB.

In other words, the so-called "additional" loss can subtract from rather than add to matched loss. Total loss can therefore be less than matched loss if a line is deliberately mismatched in the right way. A number of properties of additional loss are proved mathematically and illustrated by graphs. The author determines the limits of additional loss for all physically allowed line and load impedances. Not only should the additional loss factor not be thought of as a loss, but its reciprocal should not be thought of as an efficiency.

Common Treatment of Transmission Line Loss

It is customary in RF design engineering to assume that the characteristic impedances of transmission lines are real numbers. The assumption is poor at low frequencies but correct asymptotically at high frequencies as is evident from,

$$Z_0 = \sqrt{\frac{R + j\omega L}{G + j\omega C}} \xrightarrow[\omega \to \infty]{} \sqrt{\frac{L}{C}}. \tag{1}$$

Another way a line's characteristic impedance is real is if the line's distributed parameters R, L, G, and C satisfy Heaviside's cross-ratio condition.

$$Z_0 = \sqrt{\frac{R + j\omega L}{G + j\omega C}} \xrightarrow[\frac{R}{G} = \frac{L}{C}]{} \sqrt{\frac{L}{C}}. \tag{2}$$

If a line having real characteristic impedance is terminated with an arbitrary load impedance, it can be proved mathematically that its loss depends on just two things: the line's matched loss, and the magnitude of the reflection coefficient at the load. A formula for total loss factor widely used by radio amateurs is shown in **Table 1**. See also the **Sidebar: History of the ARRL Loss Formula.**

Although there is no question of whether practical transmission lines have real characteristic impedance (they do not), two other questions can be addressed: First, how much error does the standard formula have if a line's characteristic reactance is small compared to its characteristic resistance, but not zero? Said another way, if the phase angle of the characteristic impedance is very small, is the standard formula a good approximation? Second, are exact formulas for general line more complicated than the standard formula?

History of the ARRL Transmission Line Loss Formula and Notation

Prior to 1982, *ARRL Antenna Books* 4 (1949) through 13 (1974) published transmission line loss due to SWR in the form of graphs. The formula in **Table 1** first appeared in *Antenna Book* 14 (1982). The correct formula has appeared in every *Antenna Book* from 14 (1982) through 24 (2019). However, *Antenna Books* 15 (1988) and 16 (1991) published two different sections on the effect of SWR, where the same formula was called both "additional loss" and "total loss." The former designation was in error. The erroneous section was removed with *Antenna Book* 17 (1994).

Over the years, the *Antenna Book* presented the formula using three different notations. These may be called the "A-B-C" notation used in Antenna Books 14 through 16, the "alpha-rho" notation found in Antenna Books 15 through 17, and the current "a-rho" notation used in Antenna Books 18 through 24. Alpha "α" has a reserved meaning in transmission line theory as attenuation constant in Nepers/meter. The "alpha-rho" notation gave alpha a different meaning as the matched loss factor. Antenna Book 18 changed from "alpha-rho" to "a-rho" notation which uses the Latin un-italicized "a" instead of alpha to avoid confusion with established usage. A reader must still be watchful of fonts because italicized "*a*" in Times font is "*a*," which can be confused with alpha. *Antenna Books* 15 and 16, used rho "ρ" to mean the magnitude of a reflection coefficient. In Antenna Books 17 through 24, ρ stands for complex reflection coefficient, and $|\rho|$ is its magnitude. In the present article, upper case gamma, Γ, is used for complex reflection coefficient,

Table 1 – Formula for Total Loss Factor of Transmission Lines Having Real Z_0.

	Equation	*Valid for:*
ARRL Antenna Book, 24th ed. p. 23.13, eq. (16)	$\frac{1}{\eta} = e^{2\alpha l}\frac{1-e^{-4\alpha l}\lvert\Gamma_L\rvert^2}{1-\lvert\Gamma_L\rvert^2} = \frac{\mathrm{a}^2-\lvert\Gamma_L\rvert^2}{\mathrm{a}\left(1-\lvert\Gamma_L\rvert^2\right)}$	Z_0 real $\quad X_0 = 0$ $\mathrm{a} = e^{2\alpha l} \quad \Gamma = \frac{Z-Z_0}{Z+Z_0}$

Waves Types and Reflection Coefficients

In **[1]** the author presented loss formulas for general transmission lines. To the formulas given earlier we will add two more. The new formulas for loss are expressed in terms of reflection coefficients of power waves and "new" power waves.

Conventional voltage and current traveling waves and the normalized "scattering" waves of Montgomery, et al., **[2]** represent real power flow on a line only if the line's characteristic impedance is a real number, but if a line's characteristic impedance is not real, these wave types do not account for power flow correctly. For Youla-Kurokawa **[4]**, **[5]** power waves, the real power crossing any reference plane is the difference in the forward and reverse wave real powers, $(P_F - P_R)$. Johnston-Okoniewski **[7]** new power waves account for both real and reactive power correctly. They have the property that the real and reactive powers crossing a reference plane are the differences in the wave real powers, $(P_F - P_R)$, and reactive powers, $(Q_F - Q_R)$, respectively.

Whenever the power crossing a reference plane can be written as the difference in powers of a forward and a reverse wave, total loss factor can be written in a general form. Let the powers at a line's input and load be written as

$$\begin{aligned} P_{in} &= \lvert a_{in}\rvert^2 - \lvert b_{in}\rvert^2 \\ &= \lvert a_{in}\rvert^2\left(1-\lvert\Gamma_{in}\rvert^2\right) \\ P_L &= \lvert a_L\rvert^2 - \lvert b_L\rvert^2 \\ &= \lvert a_L\rvert^2\left(1-\lvert\Gamma_L\rvert^2\right) \quad . \end{aligned} \tag{3}$$

The total loss factor is then

$$\frac{1}{\eta} = \frac{P_{in}}{P_L} = \frac{\lvert a_{in}\rvert^2}{\lvert a_L\rvert^2}\left[\frac{1-\lvert\Gamma_{in}\rvert^2}{1-\lvert\Gamma_L\rvert^2}\right]. \tag{4}$$

In order to evaluate **(4)** it is necessary to evaluate the leading factor and, in addition, it is desirable to express the input reflection coefficient in the numerator in terms of load quantities. For conventional voltage traveling waves the required relations are simple.

$$\frac{\lvert V_{in}^+\rvert}{\lvert V_L^+\rvert} = \frac{\lvert V_L^-\rvert}{\lvert V_{in}^-\rvert} = e^{\alpha l} \quad \text{and} \quad \lvert\Gamma_{in}\rvert = e^{-2\alpha l}\lvert\Gamma_L\rvert. \tag{5}$$

Table 2 lists different wave reflection coefficients. We shall substitute the last three into **(4)**.

We consider each of three wave type separately to determine the terms in **(4)**, viz. the leading factor and the input reflection coefficient.

Montgomery-Dicke-Purcel-Colin Normalized Scattering Waves, [2] [3]

The wave quantities are related to voltage and current on the line according to

$$a = \frac{V + I Z_0}{2\sqrt{Z_0}} \qquad b = \frac{V - I Z_0}{2\sqrt{Z_0}} \tag{6}$$

$$V = (a+b)\sqrt{Z_0} \qquad I = (a-b)\sqrt{Y_0}$$

Table 2. Reflection Coefficient Summary.

Type	*Reflection Coefficient Along Line*	*Reflection Coefficient at Load*
Conventional Traveling Waves	$\Gamma(x)=\frac{Z(x)-Z_0}{Z(x)+Z_0}$	$\Gamma_L=\frac{Z_L-Z_0}{Z_L+Z_0}$
Montgomery-Dicke-Purcel Normalized Scattering Waves	$\Gamma(x)=\frac{Z(x)-Z_0}{Z(x)+Z_0}$	$\Gamma_L=\frac{Z_L-Z_0}{Z_L+Z_0}$
Youla-Kurokawa Power Waves	$\Gamma(x)=\frac{Z(x)-Z_0^*}{Z(x)+Z_0}$	$\Gamma_L=\frac{Z_L-Z_0^*}{Z_L+Z_0}$
Johnston-Okoniewski New Power Waves	$\Gamma(x)=\frac{Z(x)-\lvert Z_0\rvert}{Z(x)+\lvert Z_0\rvert}$	$\Gamma_L=\frac{Z_L-\lvert Z_0\rvert}{Z_L+\lvert Z_0\rvert}$

In matrix form the transformations are

$$\begin{bmatrix} a \\ b \end{bmatrix}=\frac{1}{2}\begin{bmatrix} \sqrt{Y_0} & \sqrt{Z_0} \\ \sqrt{Y_0} & -\sqrt{Z_0} \end{bmatrix}\begin{bmatrix} V \\ I \end{bmatrix} \tag{7}$$

$$\begin{bmatrix} V \\ I \end{bmatrix}=\begin{bmatrix} \sqrt{Z_0} & \sqrt{Z_0} \\ \sqrt{Y_0} & -\sqrt{Y_0} \end{bmatrix}\begin{bmatrix} a \\ b \end{bmatrix} \quad .$$

From the first transformation we obtain the reflection coefficient at the load as

$$\Gamma_L=\frac{b_L}{a_L}=\frac{Z_L\sqrt{Y_0}-\sqrt{Z_0}}{Z_L\sqrt{Y_0}+\sqrt{Z_0}}=\frac{Z_L-Z_0}{Z_L+Z_0} \tag{8}$$

Recall that the *ABCD* chain matrix of a transmission line is **[1, Eq. (5)]**

$$\begin{bmatrix} E_{in} \\ I_{in} \end{bmatrix}=\begin{bmatrix} \cosh\gamma l & Z_0\sinh\gamma l \\ \frac{1}{Z_0}\sinh\gamma l & \cosh\gamma l \end{bmatrix}\begin{bmatrix} E_L \\ I_L \end{bmatrix} \tag{9}$$

We combine **(8)** and **(9)** to obtain the wave transmission matrix

$$\begin{aligned}\begin{bmatrix} a_{in} \\ b_{in} \end{bmatrix}&=\frac{1}{2}\begin{bmatrix} \sqrt{Y_0} & \sqrt{Z_0} \\ \sqrt{Y_0} & -\sqrt{Z_0} \end{bmatrix}\begin{bmatrix} \cosh\gamma l & Z_0\sinh\gamma l \\ \frac{1}{Z_0}\sinh\gamma l & \cosh\gamma l \end{bmatrix}\begin{bmatrix} \sqrt{Z_0} & \sqrt{Z_0} \\ \sqrt{Y_0} & -\sqrt{Y_0} \end{bmatrix}\begin{bmatrix} a_L \\ b_L \end{bmatrix} \\ &\vdots \\ &=\begin{bmatrix} e^{\gamma l} & 0 \\ 0 & e^{-\gamma l} \end{bmatrix}\begin{bmatrix} a_L \\ b_L \end{bmatrix}\end{aligned} \tag{10}$$

and from **(10)** we obtain the quantities needed to evaluate the loss in **(4)**

$$\Gamma_{in}=\frac{b_{in}}{a_{in}}=e^{-2\gamma l}\frac{b_L}{a_L}=e^{-2\gamma l}\Gamma_L \quad \Rightarrow \quad \lvert\Gamma_{in}\rvert^2=e^{-4\alpha l}\lvert\Gamma_L\rvert^2 \tag{11}$$

$$\frac{a_{in}}{a_L}=e^{\gamma l} \quad \Rightarrow \quad \frac{\lvert a_{in}\rvert^2}{\lvert a_L\rvert^2}=e^{2\alpha l}$$

Substituting from **(11)** into **(4)**, the total loss factor is found to be

$$\frac{1}{\eta}=\frac{P_{in}}{P_L}=e^{2\alpha l}\left[\frac{1-e^{-4\alpha l}\lvert\Gamma_L\rvert^2}{1-\lvert\Gamma_L\rvert^2}\right]=\frac{\mathrm{a}^2-\lvert\Gamma_L\rvert^2}{\mathrm{a}\left(1-\lvert\Gamma_L\rvert^2\right)} \tag{12}$$

where the load reflection coefficient is given by **(8)**. This formula is the ARRL's published formula. It is exact if Z_0 is real, and an approximation otherwise.

Youla-Kurokawa Power Waves, [4] [5]

The wave quantities are related to voltage and current on the line according to

$$a=\frac{V+I\,Z_0}{2\sqrt{\mathrm{Re}(Z_0)}} \qquad b=\frac{V-I\,Z_0^*}{2\sqrt{\mathrm{Re}(Z_0)}}$$

$$V=(Z_0^*a+Z_0b)\frac{1}{\sqrt{R_0}} \qquad I=(a-b)\frac{1}{\sqrt{\mathrm{R}_0}} \tag{13}$$

In matrix form the transformations are

$$\begin{bmatrix} a \\ b \end{bmatrix}=\frac{1}{2\sqrt{R_0}}\begin{bmatrix} 1 & Z_0 \\ 1 & -Z_0^* \end{bmatrix}\begin{bmatrix} V \\ I \end{bmatrix} \tag{14}$$

$$\begin{bmatrix} V \\ I \end{bmatrix}=\frac{1}{\sqrt{\mathrm{R}_0}}\begin{bmatrix} Z_0^* & Z_0 \\ 1 & -1 \end{bmatrix}\begin{bmatrix} a \\ b \end{bmatrix}$$

From the first transformation of **(14)** we obtain the reflection coefficient at the load as

$$\Gamma_L=\frac{b_L}{a_L}=\frac{Z_L-Z_0^*}{Z_L+Z_0} \tag{15}$$

The power wave transmission matrix is found as the matrix product

$$\begin{bmatrix} a_{in} \\ b_{in} \end{bmatrix} = \frac{1}{2R_0}\begin{bmatrix} 1 & Z_0 \\ 1 & -Z_0^* \end{bmatrix}\begin{bmatrix} \cosh\gamma l & Z_0\sinh\gamma l \\ \frac{1}{Z_0}\sinh\gamma l & \cosh\gamma l \end{bmatrix}\begin{bmatrix} Z_0^* & Z_0 \\ 1 & -1 \end{bmatrix}\begin{bmatrix} a_L \\ b_L \end{bmatrix}$$

$$\vdots \qquad (16)$$

$$= \begin{bmatrix} e^{\gamma l} & 0 \\ \frac{X_0}{Z_0}\left(e^{\gamma l} - e^{-\gamma l}\right) & e^{-\gamma l} \end{bmatrix}\begin{bmatrix} a_L \\ b_L \end{bmatrix}$$

From **(16)** we obtain the quantities needed to evaluate the loss in **(4)**

$$\Gamma_{in} = \frac{b_{in}}{a_{in}} = e^{-2\gamma l}\Gamma_L + \frac{X_0}{Z_0}\left(1 - e^{-2\gamma l}\right) \quad \Rightarrow \quad \left|\Gamma_{in}\right|^2 = \Gamma_{in}\Gamma_{in}^* \qquad (17)$$

$$\frac{a_{in}}{a_L} = e^{\gamma l} \quad \Rightarrow \quad \frac{\left|a_{in}\right|^2}{\left|a_L\right|^2} = e^{2\alpha l}$$

The form of the reflection coefficient reveals the self-reflection property of power waves. Using the last line of **(17)**, the total loss factor **(4)** is therefore

$$\frac{1}{\eta} = \frac{P_{in}}{P_L} = e^{2\alpha l}\left[\frac{1 - \left|\Gamma_{in}\right|^2}{1 - \left|\Gamma_L\right|^2}\right] \qquad (18)$$

Formula **(18)** was stated without proof by Charlie Michaels, W7XC, **[6]**. We see that the W7XC formula was based on Youla-Kurokawa power waves, and its proof is given here.

Johnston-Okoniewski New Power Waves, [7], [8]

Finally we tackle new power waves following the same recipe established above. The wave quantities are related to voltage and current on the line according to

$$a = \frac{V\sqrt{Y_0^*} + I\sqrt{Z_0}}{2} \qquad b = \frac{V\sqrt{Y_0^*} - I\sqrt{Z_0}}{2} \qquad (19)$$

$$V = (a+b)\sqrt{Z_0^*} \qquad I = (a-b)\sqrt{Y_0}$$

In matrix form the transformations are

$$\begin{bmatrix} a \\ b \end{bmatrix} = \frac{1}{2}\begin{bmatrix} \sqrt{Y_0^*} & \sqrt{Z_0} \\ \sqrt{Y_0^*} & -\sqrt{Z_0} \end{bmatrix}\begin{bmatrix} V \\ I \end{bmatrix} \qquad (20)$$

$$\begin{bmatrix} V \\ I \end{bmatrix} = \begin{bmatrix} \sqrt{Z_0^*} & \sqrt{Z_0^*} \\ \sqrt{Y_0} & -\sqrt{Y_0} \end{bmatrix}\begin{bmatrix} a \\ b \end{bmatrix}$$

From the first transformation of **(20)** we obtain the reflection coefficient at the load as

$$\Gamma_L = \frac{b_L}{a_L} = \frac{Z_L\sqrt{Y_0^*} - \sqrt{Z_0}}{Z_L\sqrt{Y_0^*} + \sqrt{Z_0}} = \frac{Z_L - \left|Z_0\right|}{Z_L + \left|Z_0\right|} \qquad (21)$$

The new power wave transmission matrix is found as a matrix product

$$\begin{bmatrix} a_{in} \\ b_{in} \end{bmatrix} = \frac{1}{2}\begin{bmatrix} \sqrt{Y_0^*} & \sqrt{Z_0} \\ \sqrt{Y_0^*} & -\sqrt{Z_0} \end{bmatrix}\begin{bmatrix} \cosh\gamma l & Z_0\sinh\gamma l \\ \frac{1}{Z_0}\sinh\gamma l & \cosh\gamma l \end{bmatrix}\begin{bmatrix} \sqrt{Z_0^*} & \sqrt{Z_0^*} \\ \sqrt{Y_0} & -\sqrt{Y_0} \end{bmatrix}\begin{bmatrix} a_L \\ b_L \end{bmatrix}$$

$$\vdots \qquad (22)$$

$$= \begin{bmatrix} \left|k_p^2\right|e^{\gamma l} + \left|k_n^2\right|e^{-\gamma l} & k_p^* k_n e^{\gamma l} + k_p k_n^* e^{-\gamma l} \\ k_p k_n^* e^{\gamma l} + k_p^* k_n e^{-\gamma l} & \left|k_n^2\right|e^{\gamma l} + \left|k_p^2\right|e^{-\gamma l} \end{bmatrix}\begin{bmatrix} a_L \\ b_L \end{bmatrix}$$

where k_p and k_n are auxiliary variables defined by

$$k_p = \frac{1}{2}\left(\frac{Z_0^*}{\left|Z_0\right|} + 1\right) \quad \text{and} \quad k_n = \frac{1}{2}\left(\frac{Z_0^*}{\left|Z_0\right|} - 1\right) \qquad (23)$$

From **(22)** we obtain the quantities needed to evaluate the loss in **(4)**

$$\Gamma_{in} = \frac{b_{in}}{a_{in}} = \frac{\Gamma_L\left(\left|k_n^2\right|e^{\gamma l} + \left|k_p^2\right|e^{-\gamma l}\right) + k_p k_n^* e^{\gamma l} + k_p^* k_n e^{-\gamma l}}{\Gamma_L\left(k_p^* k_n e^{\gamma l} + k_p k_n^* e^{-\gamma l}\right) + \left|k_p^2\right|e^{\gamma l} + \left|k_n^2\right|e^{-\gamma l}}$$

$$= \frac{k_n^*\left(k_p + \Gamma_L k_n\right)e^{\gamma l} + k_p^*\left(\Gamma_L k_p + k_n\right)e^{-\gamma l}}{k_p^*\left(k_p + \Gamma_L k_n\right)e^{\gamma l} + k_n^*\left(\Gamma_L k_p + k_n\right)e^{-\gamma l}} \qquad (24)$$

$$\frac{a_{in}}{a_L} = \Gamma_L\left(k_p^* k_n e^{\gamma l} + k_p k_n^* e^{-\gamma l}\right) + \left|k_p^2\right|e^{\gamma l} + \left|k_n^2\right|e^{-\gamma l}$$

$$= k_p^*\left(k_p + \Gamma_L k_n\right)e^{\gamma l} + k_n^*\left(\Gamma_L k_p + k_n\right)e^{-\gamma l}$$

Further algebraic expansion, while possible, does not lead to a simple compact form. The total loss factor is obtained by substituting **(24)** into **(4)**,

$$\frac{1}{\eta} = \frac{P_{in}}{P_L} = \frac{\left|a_{in}\right|^2}{\left|a_L\right|^2}\left[\frac{1 - \left|\Gamma_{in}\right|^2}{1 - \left|\Gamma_L\right|^2}\right] \qquad (25)$$

This is best done numerically for specific cases.

Formulas for Loss

Table 3 is a revised list of general loss formulas for transmission lines that have complex Z_0. This table revises the table given in **[1]**. The following changes are noted. The Jackson and King-Mimno-Wing formulas were checked and found to be restricted, i.e. not general for complex Z_0. Accordingly, these formulas have been dropped from the table. New formulas are added corresponding to the *Y-K* power wave and *J-O* new power wave formulations of loss. All of the formulas in the table have been evaluated over a wide range of complex characteristic impedances and load impedances. The formulas are all in agreement to machine accuracy with one caveat: King's general formula, **[9]**, **[10]**, in row 6 is problematic because King's parameters ρ and Φ require computing the inverse hyperbolic

cotangent of the normalized load impedance Z_L/Z_0. However, the inverse hyperbolic cotangent function has a branch cut on the real interval [−1, +1]. Consequently King's formula cannot be used for matched loads, anti-matched loads, or anything in between (e.g. short circuit loads). King's formula is an example of a formula that is correct for all cases except ones we are interested in! Kennelly's formula, **[11]**, in row 7 should have a similar problem. Kennelly's parameter θ' requires computing the inverse hyperbolic tangent of the normalized load impedance, which has branch cuts on the open intervals $(-\infty, -1]$ and $[+1, \infty)$. Consequently, Kennelly's formula should not be used if the load is a real multiple of Z_0. Knowing this, one should use Kennelly's and King's formulas with caution. The other formulas in the table are well behaved.

Some comments are in order concerning Macalpine's formula in row 5,

$$\frac{1}{\eta} = e^{2\alpha l}\left[\frac{1-|\Gamma_{in}|^2 - 2|\Gamma_{in}|\left(\frac{X_0}{R_0}\right)\sin 2\psi_{in}}{1-|\Gamma_L|^2 - 2|\Gamma_L|\left(\frac{X_0}{R_0}\right)\sin 2\psi_L}\right]. \quad (26)$$

William Macalpine worked at Federal Telecommunications Laboratories. He published his formula in 1953 **[12]**. His formulas for power and efficiency have appeared in every Federal/ITT handbook from the 1956 4th edition **[13]** to the present 9th edition **[14]**. The first factor $e^{2\alpha l}$ is the matched loss factor, and the expression it multiplies in brackets is the "additional loss due to SWR." By setting $X_0 = 0$ and using the symbol "a" for the matched loss factor, Macalpine's formula simplifies to the ARRL formula in **Table 1**.

Table 3 – Exact Formulas for Total Loss Factor of Transmission Lines Having Complex Z_0.

Author	*Total Loss Factor*	*Claims*
S.D. Stearns, K6OIK ARRL Pacificon 2014	$\frac{1}{\eta} = \frac{R_{in}}{R_L}\left\lvert\cosh\gamma l + \frac{Z_L}{Z_0}\sinh\gamma l\right\rvert^2 = \frac{R_{in}}{R_L}\frac{1}{\left\lvert\cosh\gamma l - \frac{Z_{in}}{Z_0}\sinh\gamma l\right\rvert^2}$	General, where $\gamma = \alpha + j\beta$
S.D. Stearns, K6OIK, 2020 [1]	$\frac{1}{\eta} = \frac{G_{in}}{G_L}\left\lvert\cosh\gamma l + \frac{Z_0}{Z_L}\sinh\gamma l\right\rvert^2 = \frac{G_{in}}{G_L}\frac{1}{\left\lvert\cosh\gamma l - \frac{Z_0}{Z_{in}}\sinh\gamma l\right\rvert^2}$	General, where $\gamma = \alpha + j\beta$
Johnston-Okoniewski New Power Waves, 2016, 2019.	$\frac{1}{\eta} = \frac{\lvert a_{NP,in}\rvert^2}{\lvert a_{NP,L}\rvert^2}\frac{1-\lvert\Gamma_{in}\rvert^2}{1-\lvert\Gamma_L\rvert^2}$	General, where $\Gamma = \frac{Z-\lvert Z_0\rvert}{Z+\lvert Z_0\rvert}$
Youla-Kurokawa Power Waves 1961, 1965.	$\frac{1}{\eta} = e^{2\alpha l}\frac{1-\lvert\Gamma_{in}\rvert^2}{1-\lvert\Gamma_L\rvert^2}$	General, where $\Gamma = \frac{Z-Z_0^*}{Z+Z_0}$
W. W. Macalpine, Trans. AIEE, July 1953, Eq. 13	$\frac{1}{\eta} = e^{2\alpha l}\frac{1-\lvert\Gamma_{in}\rvert^2 - 2\lvert\Gamma_{in}\rvert\left(\frac{X_0}{R_0}\right)\sin 2\psi_{in}}{1-\lvert\Gamma_L\rvert^2 - 2\lvert\Gamma_L\rvert\left(\frac{X_0}{R_0}\right)\sin 2\psi_L}$	General, where $\Gamma = \lvert\Gamma\rvert e^{j2\psi}$
R.W.P. King J.A.P., Nov. 1943, p. 593, Eq. 84 and 1955, ch. 4, § 6, Eq. 10	$\frac{1}{\eta} = \frac{\sinh 2(\alpha l + \rho) - \phi\sin 2(\beta l + \Phi)}{\sinh 2\rho - \phi\sin 2\Phi}$	General, where $\coth(\rho + j\Phi) = \frac{Z_L}{Z_0}$ $Z_0 = R_0(1 - j\phi)$
A. E. Kennelly, 1912 p. 117, Eq. 202d	$\frac{1}{\eta} = \frac{R_{in}}{R_L}\left\lvert\frac{\sinh\gamma l + \frac{Z_L}{Z_0}\cosh\gamma l}{\tanh(\gamma l + \theta')}\right\rvert^2$	General, where $\tanh\theta' = \frac{Z_L}{Z_0}$

Does It Matter?

We have spent some effort to arrive at exact formulas for transmission line loss. Was the effort worth it? The reader may rightly ask whether the ARRL formula in **Table 1** is good enough. After all, the characteristic impedance of any practical transmission line is very nearly a real number at amateur frequencies. What does it matter if a line is slightly reactive by less than an ohm? This question has been asked before. The answer has two aspects. A devil's advocate may counter with the question, "Why continue to use an approximate formula for loss when exact ones are available?" After all, the exact formulas in the first five rows of **Table 3** are no harder to compute than the ARRL formula. So why not use them? If one is going to calculate, at least get the formula right, and for that matter, get the right formula.

The second aspect concerns accuracy. How great is the error that results from using an inexact formula for loss? We shall answer this question by showing three examples in which the lines and loads correspond to realistic situations that may be encountered. The first two examples show that the total loss can be greater than that predicted by the ARRL formula. Thus that formula can underestimate the actual loss of a terminated line. The third example is Paradox 5. It shows that the total loss can be less than that predicted by the ARRL formula, less even than the matched loss in certain cases. Thus the ARRL formula can either underestimate or overestimate the actual loss of a terminated line.

Example 1: Total Loss Greater than Predicted by ARRL Loss Formula

The first example comes from R. Dean Straw, N6BV, in the revised 2014 documentation for *TLW* **[15]**. The author presented an analysis of this example at Pacificon 2014 **[16]**. The parameters of the example are in **Table 4A**.

Table 4A – Example #1 analysis parameters.

Line type	Wireman #551, 450 Ω window line, solid #18 AWG copper-clad
Length	100 feet
Frequency	1.83 MHz
Attenuation alpha	0.095 dB/100 feet
Velocity factor	0.915
Z_0 resistance R_0	402.75 Ω
Z_0 reactance X_0	–3.45 Ω
Load resistance R_L	4.5 Ω
Load reactance X_L	–1,673 Ω

Table 4B – Line Loss for Input Power of 1,500 watts.

	Table 1 formula (for Z_0 real)	Table 3 formulas (for arbitrary Z_0)	TLW software
Matched loss	0.095 dB	0.095 dB	0.095 dB
Additional loss due to SWR	7.125 dB	13.179 dB	13.182 dB
Total line loss	7.220 dB	13.274 dB	13.277 dB
Power delivered to load	284.5 W	70.6 W	70.5 W
Power dissipated in line	1215.5 W	1429.4 W	1429.5 W

According to N6BV, the load is a 100-foot long, center-fed dipole, 50 feet above average ground. Apparently the load impedance may also correspond to an 81-foot cage dipole having 32-inch diameter in free space **[16]**, similar in size to the dipoles used in the Woodpecker, the Duga over-the-horizon radar near Chernobyl. **Table 4B** compares the loss calculations assuming 1,500 W is delivered to the line's input.

The ARRL loss formula underestimates line loss by more than 6 dB. Dan Maguire, AC6LA, computed this example for line lengths out to 500 feet. **Figure 1** shows the total loss versus line length as computed by several methods. The exact total loss is the top curved line, computed by three formulas all in perfect agreement. The middle line is the ARRL loss formula, and the bottom line is the matched loss. The ARRL formula underestimates total loss by as much as 7 dB when the line length is 160 feet.

It is evident that the ARRL loss formula can be inaccurate for even small departures from real Z_0 ($X_0 < 0.009\ R_0$); its predicted loss can be significantly in error. We conclude that even for low-loss window line, ignoring the seemingly small imaginary part of Z_0 of practical transmission lines can give large error in predicted delivered power using the **Table 1** formula. It is best to use one of the exact formulas of **Table 3** even if the line reactance is small and seems negligible.

Example 2: Total Loss Periodically Equal to That Predicted by ARRL Loss Formula

The second example is from Dan Maguire, AC6LA, and appears on his web site **[17]**. Consider RG-8X coax at 3.5 MHz terminated with $Z_L = 54.52 - j\ 62.84\ \Omega$. **Figure 2** shows the total loss computed by several methods versus line length. Again, the exact total loss is the curved top line. The middle line is the ARRL loss formula, and the bottom straight line is the matched loss.

We observe the error of the ARRL formula error, i.e. the difference between the top and middle curves, is periodic as line length varies. The ARRL formula agrees with the exact total loss at half wavelength multiples. There are two conditions under which the ARRL total loss formula (**Table 1**) is exact. The first condition is when Z_0 is real. However, there is another condition under which the ARRL formula is exact, and for complex Z_0 lines. If the characteristic impedance Z_0 and load impedance Z_L have equal phase angles, so the reflection coefficient at the load Γ_L is real, then the ARRL formula is exact at locations along a line where the reflection coefficient $\Gamma(x)$ toward the load is real for at these locations we have $\psi_{in} = \psi_L = 0$. The phenomenon is evident in **Figure 2** where the exact total loss curve and the ARRL loss line make periodic contact every half wavelength.

Paradox 5: Total Loss Less than Matched Loss

In **[1]** it was claimed that the minimum total loss of a terminated line is the line's matched loss only if Z_0 is real *but not necessarily otherwise*. We demonstrate the truth of the last part of the statement. As in Example 2, consider again RG-8X coax at 3.5 MHz terminated now with the conjugate load $Z_L = 54.52 + j\ 62.84\ \Omega$. **Figure 3** shows the total loss computed versus line length. The exact total loss is the curved (middle and dashed) lines, this time computed by four methods, all in perfect agreement. The upper straight line is the ARRL loss formula, and the lower straight line is the matched loss. For transmission line lengths

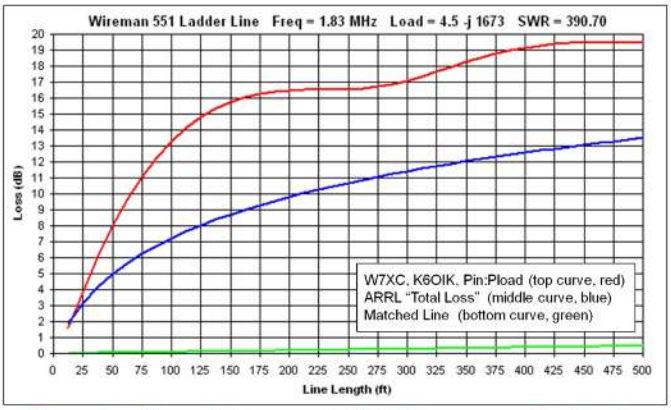

Figure 1 — Example 1: computed total loss versus line length.

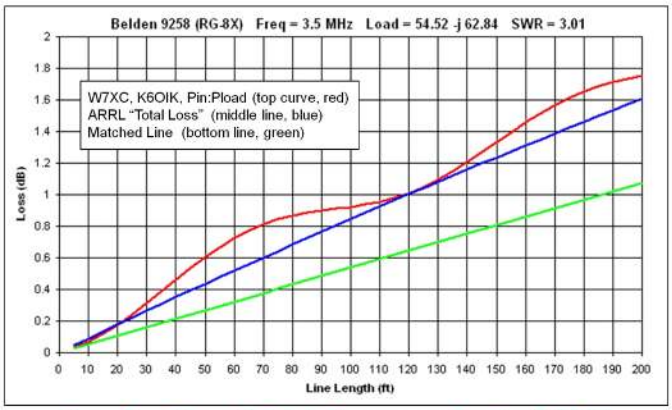

Figure 2 — Example 2: total loss versus length of RG-8X terminated with complex load.

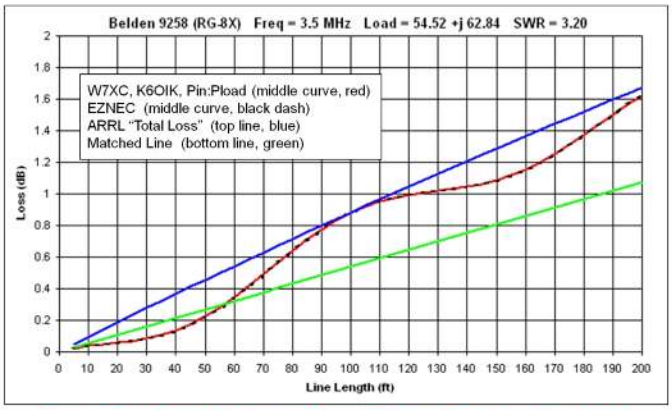

Figure 3 — Total loss when terminated with a complex load.

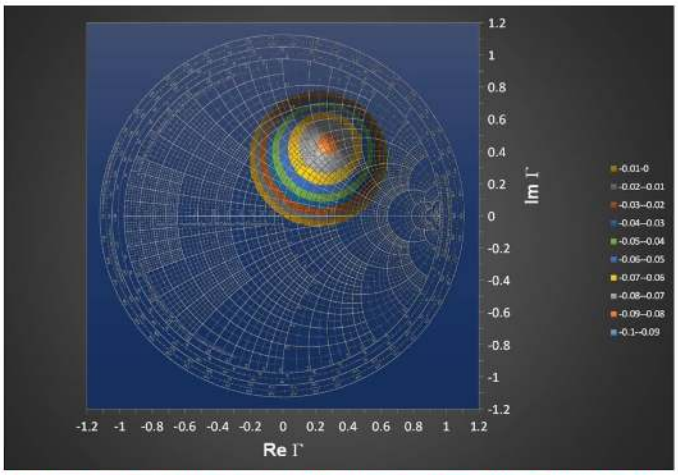

Figure 4 — Additional loss in dB, superimposed on a Smith Chart.

between 10 and 56 feet, the exact total loss is less than the matched loss. In other words, the additional loss due to SWR is negative for line lengths between 10 and 56 feet!

How can this be? When Z_0 is complex, the last terms in the numerator and denominator of Macalpine's formula (26) must be included. For certain combinations of line length and load, the "additional loss" factor is less than unity. Suppose a line has $X_0 < 0$ (true for most lines). Choose the load such that $\sin(2\psi_L)$ is positive, and choose a short line length for which $\sin(2\psi_{in})$ is negative. Under these conditions the additional loss factor can be less than unity.

Let's examine this example more closely. From **Figure 3** the total loss is below the matched loss by the greatest amount at 36.15 feet. In decibels additional loss equals total loss minus matched loss. Additional loss is negative and minimum at 36.15 feet. We fix the line at this length and investigate load impedances near the assumed load of $54.52 + j\ 62.84\ \Omega$. **Figure 4** shows the result. The bull's-eye pattern is a pseudo-color plot of additional loss in dB plotted in the reflection coefficient plane. A Smith chart is superimposed for reference. Additional loss is shown in 0.01 dB bins from –0.09 to zero dB. The minimum value of additional loss is at the center of the bull's-eye and is found to be –0.0817 dB. This value occurs at a load reflection coefficient of $\Gamma_L = 0.28 + j\ 0.45$, which corresponds to a normalized load impedance of $z_L = 0.9975 + j\ 1.24843$, or a load impedance of $Z_L = 52.39 + j\ 62.74\ \Omega$. The load assumed in **Figure 3**, $Z_L = 54.52 + j\ 62.84\ \Omega$, is very close to that which gives minimum additional loss. If the line length is increased from 36.15, the bull's-eye moves, revolving counterclockwise, and the minimum value changes. Knowing this, one can choose a load impedance matching strategy which involves adjusting line length or load impedance presented to the line to advantage.

This example is realistic. The line is RG-8X, the lengths in question, 20 to 50 feet, are reasonable, and the slightly inductive load is not very mismatched. More extreme examples are possible. We conclude that for practical transmission line which has a complex characteristic impedance, maximum efficiency does not always equal matched efficiency, nor is it necessarily achieved with a matched load or in the absence of a reverse traveling wave. Maximum efficiency can exceed matched efficiency, and minimum loss can be less than matched loss for certain combinations of line length and load impedance. Moreover, as can be seen in **Figure 3**, the slope of the total loss curve, i.e. the partial derivative with respect to line length, can oscillate. The minimum slope can be near zero. When the slope is near zero, one can add small amounts of length with almost no increase in loss. In this example we've shown how to get almost a tenth of a decibel for free by transmission line trickery. But can we do better?

The Limits of Loss

The examples show that the exact total loss factor can be either greater or less than that given by the ARRL loss formula, less even than a line's matched loss. A reasonable question to ask is how much can the additional loss factor deviate from unity in either direction. We won't answer the question of how large the additional loss factor can be because the answer is obvious: infinity. A pure reactance load accepts no real power from a line. Example 1 used this fact. We shall answer the question of how small the additional loss factor can be if all possible characteristic impedances, load impedances, and line lengths are considered. We shall show it is far more than mere tenths of a dB negative.

We first review some properties of Smith charts. A Smith chart

is a functional mapping of the impedance plane to the reflection coefficient plane. The mapping is one-to-one and invertible. The shaded regions in **Figure 5** show how the right half of the impedance plane maps to the interior of the unit disk to give the familiar Smith chart. The semicircle maps to the vertical axis inside the disk. The left half of the impedance plane maps to the exterior of the disk, outside of the Smith chart.

Often impedances are normalized by dividing by the characteristic impedance. If impedances in the right half of the impedance plane are normalized by a real characteristic impedance, they map to the interior of the unit disk, i.e. the interior of the Smith chart, as shown. However if the impedances are normalized by a complex characteristic impedance, the normalization rotates the half plane by an angle that is the negative of the characteristic impedance phase angle, and the rotated half plane maps to a different region of the complex plane.

The phase angle of a characteristic impedance is restricted to the quadrant $\pm\pi/4$ radians ($\pm 45°$) **[1, p. 13]**. **Figure 6** shows the limiting case when the phase angle of the complex normalizing impedance is $-45°$ or $X_0/R_0 = -1$. Load impedances initially in the right half plane, upon normalization, map to a rotated impedance half-plane, which in turn maps to the interior of a Q circle. When normalizing by a complex impedance $Z_0 = R_0 + j\,X_0$, the ratio X_0/R_0 is $1/Q$ and R_0/X_0 is Q. [To avoid confusion with conventional usage, it is best to forget the customary definition of Q as 2π times a ratio of the stored energy to energy dissipated in a cycle, and regard Q simply as a mathematical variable convenient for describing circles on a Smith chart.] A constant Q circle in the reflection coefficient plane has its center at

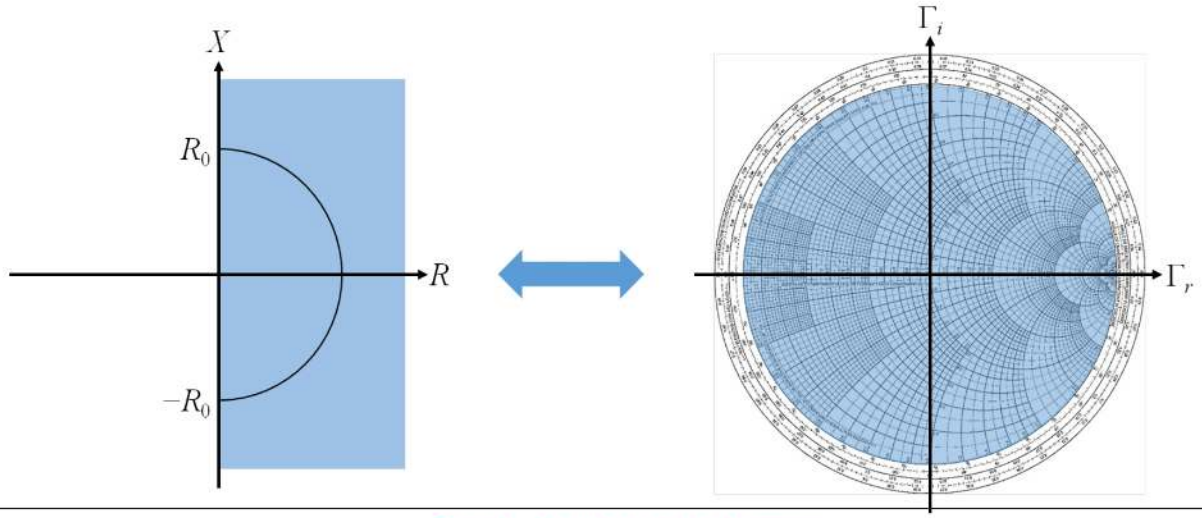

Figure 5 — Smith chart region mapping.

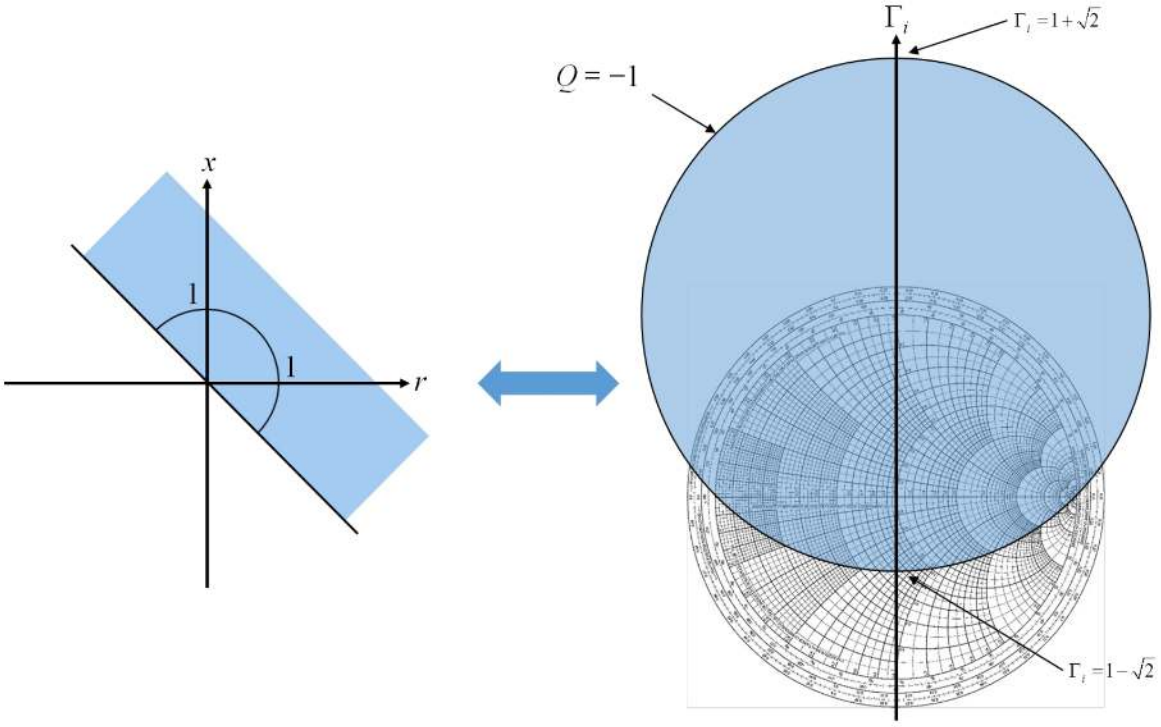

Figure 6 — Smith chart region mapping with complex impedance normalization.

$(0, -1/Q)$, and radius $\sqrt{1+1/Q^2}$. In this case, $Q = -1$, the circle is centered at (0, 1), and its radius is $\sqrt{2}$. The extremes of reflection coefficient magnitude occur on the central vertical axis for which the real part of Γ is zero, and are $1+\sqrt{2}$ and $1-\sqrt{2}$ respectively. Thus at its magnitude extremes, the reflection coefficient is imaginary.

The rotated half plane on the left side of **Figure 6** can lie at any angle between ±45° depending on the complex characteristic impedance used for normalization. As the half plane rotates clockwise from the position shown, the Q circle drops, like the Times Square ball, and shrinks. When the half plane coincides with the right half plane, the shaded disk coincides with the interior of the Smith chart. As the half plane continues to rotate clockwise, the Q circle descends and grows larger until –45° is reached. At this point the situation is the mirror image of the starting position, and the shaded region is the interior of the $Q = +1$ circle.

When examining questions of the limits of loss, it is important to restrict consideration to passive load impedances. On the Smith chart this means only points inside the appropriate Q circle should be considered. Points outside the circle correspond to active load impedances, and the loss formulas do not apply.

In Macalpine's formula **(26)** the phase angle $2\psi_L$ of the load reflection coefficient depends on the load impedance while the phase angle $2\psi_{in}$ of the input reflection coefficient depends on the load impedance and the line length. If the line length is an odd multiple of a quarter wave, then $\sin(2\psi_{in})$ will be +1 whenever $\sin(2\psi_L)$ is –1 and vice versa. Hence the numerator of **(26)** will be maximum when the denominator is minimum and vice versa.

The following definitions and identities will prove useful.

$$\begin{aligned}
\Gamma_{r,in} &= \mathrm{Re}\,\Gamma_{in} = |\Gamma_{in}|\cos 2\psi_{in} \\
\Gamma_{i,in} &= \mathrm{Im}\,\Gamma_{in} = |\Gamma_{in}|\sin 2\psi_{in} \\
\Gamma_{r,L} &= \mathrm{Re}\,\Gamma_{L} = |\Gamma_{L}|\cos 2\psi_{L} \\
\Gamma_{i,L} &= \mathrm{Im}\,\Gamma_{L} = |\Gamma_{L}|\sin 2\psi_{L} \\
|\Gamma_{in}| &= e^{-2\alpha l}|\Gamma_L|
\end{aligned} \tag{27A}$$

$$\begin{aligned}
\Gamma_{in} &= e^{-2\gamma l}\Gamma_L \\
&= e^{-2\alpha l}\left(\cos 2\beta l - j\sin 2\beta l\right)\left(\Gamma_{r,L} + j\,\Gamma_{i,L}\right) \\
&= e^{-2\alpha l}\left[\begin{array}{l}\left(\Gamma_{r,L}\cos 2\beta l + \Gamma_{i,L}\sin 2\beta l\right) + \\ j\left(\Gamma_{i,L}\cos 2\beta l - \Gamma_{r,L}\sin 2\beta l\right)\end{array}\right] \\
\Gamma_{r,in} &= e^{-2\alpha l}\left(\Gamma_{r,L}\cos 2\beta l + \Gamma_{i,L}\sin 2\beta l\right) \\
\Gamma_{i,in} &= e^{-2\alpha l}\left(\Gamma_{i,L}\cos 2\beta l - \Gamma_{r,L}\sin 2\beta l\right)
\end{aligned} \tag{27B}$$

Converting reflection coefficients in **(26)** from polar to Cartesian form, the additional loss factor may be written as

$$\begin{aligned}
\frac{\eta_{matched}}{\eta} &= \frac{1-|\Gamma_{in}|^2 - \dfrac{2}{Q}\Gamma_{i,in}}{1-|\Gamma_L|^2 - \dfrac{2}{Q}\Gamma_{i,L}} \\
&= e^{-4\alpha l}\frac{|\Gamma_L|^2 + \dfrac{2e^{2\alpha l}}{Q}\left(\Gamma_{i,L}\cos 2\beta l - \Gamma_{r,L}\sin 2\beta l\right) - e^{4\alpha l}}{|\Gamma_L|^2 + \dfrac{2}{Q}\Gamma_{i,L} - 1}
\end{aligned} \tag{28}$$

Formula **(28)** is general. The denominator defines a paraboloid. The paraboloid is zero on a circle in the complex plane, the Q circle discussed above. Accordingly, **(28)** has a ring singularity. It is infinite on the circle. The numerator of **(28)** also defines a paraboloid, which is zero on a different circle. Evidently the matched loss is sufficiently great that this zero circle is large enough to completely contain the ring singularity circle. Otherwise the additional loss factor could be negative inside the disk which is impossible for passive termination impedances.

We consider a special case of **(28)** by making two assumptions:
- $|Z_L| = |Z_0|$, so the load impedance is on the semicircle in **Figure 6**, $\Gamma_{r,L} = 0$ and Γ_L is imaginary.
- The line length is a quarter wave, $\beta\, l = \pi/2$, so $\cos(2\beta l) = -1$ and $\sin(2\beta l) = 0$.

Essentially we are taking a slice through the surface defined by **(28)** along the imaginary reflection coefficient axis. The slice corresponds to the impedance constraint $|Z_L| = |Z_0|$. Upon simplifying and factoring we obtain

$$\begin{aligned}
\frac{\eta_{matched}}{\eta} &= e^{-4\alpha l}\frac{\Gamma_{i,L}^2 - \dfrac{2e^{2\alpha l}}{Q}\Gamma_{i,L} - e^{4\alpha l}}{\Gamma_{i,L}^2 + \dfrac{2}{Q}\Gamma_{i,L} - 1} \\
&= e^{-4\alpha l}\frac{\left(\Gamma_{i,L} - \left(\dfrac{1}{Q} - \sqrt{1+\dfrac{1}{Q^2}}\right)e^{2\alpha l}\right)\left(\Gamma_{i,L} - \left(\dfrac{1}{Q} + \sqrt{1+\dfrac{1}{Q^2}}\right)e^{2\alpha l}\right)}{\left(\Gamma_{i,L} - \left(-\dfrac{1}{Q} - \sqrt{1+\dfrac{1}{Q^2}}\right)\right)\left(\Gamma_{i,L} - \left(-\dfrac{1}{Q} + \sqrt{1+\dfrac{1}{Q^2}}\right)\right)}
\end{aligned} \tag{29}$$

The factored form reveals two poles and two zeros which are on the imaginary axis. Poles are on the disk boundary at the top and bottom of the circle and are due to the ring singularity. Similarly the zeros are due to the zero circle.

We evaluate **(29)** for the extreme case shown in **Figure 6**, for which the phase angle of Z_0 is –45° so $X_0/R_0 = 1/Q = -1$. Given the phase angle of Z_0 is –45°, the phase angle of the propagation constant γ must be +45° because distributed parameters G (conductance) and L (inductance) must be zero. Hence the attenuation constant α equals the phase constant β, and the matched loss factor is

$$\mathrm{a} = e^{2\alpha l} = e^{2\beta l} = e^{\pi} = 23.140\ldots \tag{30}$$

Upon substituting $Q = -1$ and **(30)** into **(29)**, the additional loss factor is found to be

$$\frac{\eta_{matched}}{\eta} = e^{-2\pi}\frac{\left(\Gamma_{i,L} - \left(-1-\sqrt{2}\right)e^{\pi}\right)\left(\Gamma_{i,L} - \left(-1+\sqrt{2}\right)e^{\pi}\right)}{\left(\Gamma_{i,L} - \left(1-\sqrt{2}\right)\right)\left(\Gamma_{i,L} - \left(1+\sqrt{2}\right)\right)} \tag{31}$$

Poles and zeros are on the imaginary axis, with poles at –0.4142 and 2.1412 and zeros at –55.867 and 9.5851. We observe the poles do indeed lie between the zeros, which guarantees the additional loss factor is positive.

Passive impedances map to the semicircle in **Figure 6** and thence to the interval $1-\sqrt{2} < \Gamma_{i,L} < 1+\sqrt{2}$, inside the $Q = -1$ circle. The additional loss is infinite at the endpoints. Evaluating **(31)** at $\Gamma_{i,L} = 1$ (the center of the circle), we discover

$$\frac{\eta_{matched}}{\eta} = e^{-2\pi}\frac{\left(1-\left(-1-\sqrt{2}\right)e^{\pi}\right)\left(1-\left(-1+\sqrt{2}\right)e^{\pi}\right)}{\left(\sqrt{2}\right)\left(-\sqrt{2}\right)}$$
$$= \frac{1}{535.49}\left(\frac{56.867\times 8.5851}{2}\right) \qquad (32)$$
$$= 0.45585 \quad (-3.41\ \text{dB})$$

The additional loss factor is less than unity (or –3.41 dB) at the center of the circle, but this is not necessarily minimum. The question of what is the minimum additional loss factor over the interval is answered by **Figure 7**, a graph of the additional loss along the imaginary axis.

Figure 7 shows the additional loss along a vertical slice down the center of the Smith chart. The loss goes to infinity at –0.414 and 2.414. The first main thing to note is that the additional loss is less than unity (negative in dB) over a broad range that extends from zero to 2.09. This means that almost the entire semicircle of normalized load impedances in **Figure 6** give sub-unity additional loss factor. Second, the minimum does not occur at the exact center of the passive load circle but at $\Gamma_L = 0 + j\ 1.1$, which corresponds to a normalized load impedance of $z_L = -0.09502 + j\ 0.99548$, or a load impedance of $Z_L = R_0\ (0.90046 + j\ 1.0905)\ \Omega$. The minimum additional loss is –3.43 dB, a little bit less than calculated in **(32)** at the center of the circle.

Perhaps more revealing is **Figure 8**, which shows the additional loss factor in 0.25 dB bins from –3.5 dB to zero dB, plotted in reflection coefficient plane. Passive load impedances are inside the white $Q = -1$ circle centered at (0, 1) radius $\sqrt{2}$. Several things are evident. First, for quarter-wave line, the loss surface has left-right symmetry. Second, for quarter-wave line the minimum of the additional loss does indeed occur on the central vertical axis. So the cut through the surface in **Figure 7** does indeed capture the minimum, at least for quarter-wave line, which in this case is –3.43 dB. Third, the bull's-eye pattern is slightly asymmetric top-to-bottom. The minimum occurs slightly above center in agreement with **Figure 7**.

Loss Factors as Efficiencies

Power transmission efficiency is the reciprocal of total loss factor **[1]**. Accordingly it can be written as a product of factors: the reciprocal of matched loss factor (so called matched efficiency) times the reciprocal of the additional loss factor. Paradox 5 makes clear the reciprocal of the additional loss factor can exceed 100%. In the last example, it is 220%. Hence the reciprocal of the additional loss factor should not be interpreted as an efficiency lest we admit passive systems are not bound to the principle of energy conservation.

When an efficiency can be written as a product of factors, one must resist the temptation to call the individual factors efficiencies unless such an interpretation is physically justified. Just because an efficiency can be written as a product of factors does not make the factors efficiencies. To those who dissent, I point out that to an efficiency of the form

$$\eta_{total} = \eta_1 \cdot \eta_2 \cdot \eta_3 \qquad (28)$$

one may introduce extra factors willy-nilly to obtain, for example,

$$\eta_{total} = \eta_1 \cdot 2 \cdot \eta_2 \cdot 0.5 \cdot \eta_3\ . \qquad (29)$$

To insist that all factors are efficiencies leads to nonsense. Such is the plight of "additional loss due to SWR." It is not a real loss any more than its reciprocal is an efficiency. Unfortunately names can be deceiving.

Concluding Remarks

We reviewed existing formulas for the exact computation of the total loss of a terminated general uniform transmission line and proved new ones. We gave a simple proof of the ARRL loss formula. We proved the W7XC formula by deriving it from Youla-Kurokawa power wave theory, thereby resolving the mystery of the W7XC formula origin and correctness. We derived a new loss formula based on Johnston-Okoniewski new power wave theory. We gave examples to show that the ARRL loss formula can significantly underestimate and overestimate total loss, and may do so under reasonable conditions which an amateur may encounter in practice. Finally, we presented Paradox 5, which showed the "additional loss due to SWR" in certain cases can be negative in dB, so a line's total loss is less than its matched loss. We explored just how small the additional loss can it be if Z_0 and Z_L are arbitrary, and gave an example in which the additional loss of a quarter-wave line is –3.43 dB. We did not prove that this is the most negative value possible; although we suspect this is the case. Of greater interest than how negative the additional loss can be is the question of how to exploit this phenomenon to cancel as much of a line's matched loss as possible. Many questions remain that space does not permit to be explored in this article.

- Do the extreme Z_0 cases for which $X_0/R_0 = 1/Q = \pm 1$ lead to the globally smallest possible values for the additional loss?
- For characteristic impedances for which $|X_0/R_0| < 1$, how small can the additional loss be made?
- For characteristic impedances for which $|X_0/R_0| < 1$, how much matched loss can be cancelled, and what are the conditions?
- Can the slope of additional loss with respect to line length be less than the negative of the attenuation constant such that an incremental increase of a line's length causes total loss to decrease?

In examining and partially answering such questions, have we opened Pandora's Box? Will new philosophies for impedance matching emerge — methods that can deliver a bit more power to a load by the careful trimming of line length and deliberate mismatching a load? Time will tell.

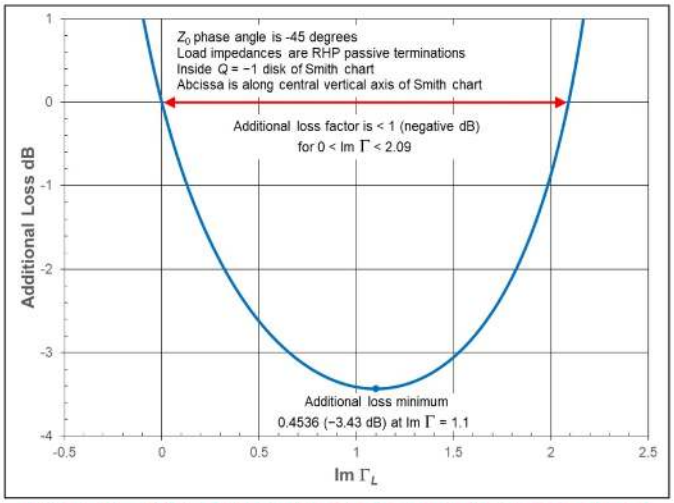

Figure 7 — Additional loss in dB versus imaginary part of load reflection coefficient.

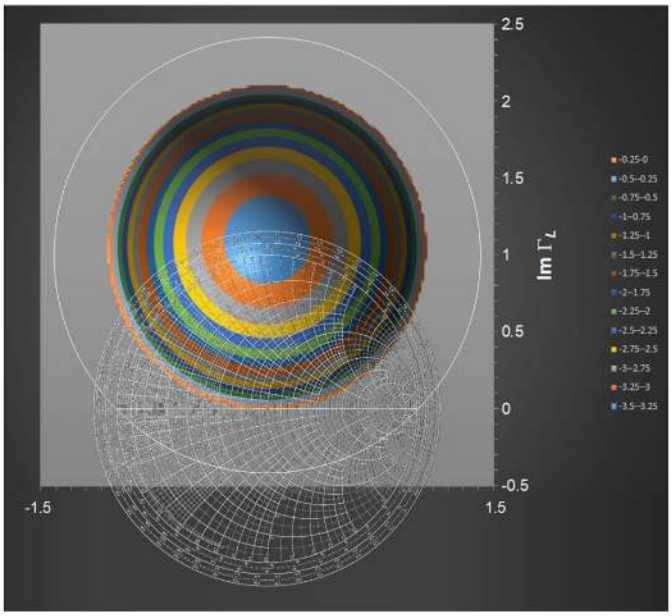

Figure 8 — Additional loss in dB for quarter-wave line $X_0/R_0 = 1/Q = -1$.

It should be mentioned that the ideas here are unrelated to conjugate matching and the maximum power transfer theorem. Our matching philosophy is that a load and line should be designed as a system for minimum total loss. Source impedance plays no role. In amateur transmitting systems, the FCC rules for the Amateur Service impose regulatory limits on transmitter output power not on "available" power. The maximum power transfer theorem is irrelevant given how the FCC regulations about amateur transmitter power are worded. Once power is delivered to the line, it is line loss alone that determines the amount of power that is delivered to the transmitting antenna.

Making a dipole non-resonant and slightly long, or inductive, can have two serendipitous effects: greater dipole gain from the extra length, and transmission line loss less than matched loss from the Paradox 5 effect. If the impedance match criterion is maximum EIRP, then the optimal impedance match of antenna to line is not a perfect match nor a conjugate match. One can jointly optimize antenna length/gain and complex reflection coefficient presented to a line. The optimal maximum EIRP solution requires a reverse wave on the line and, hence, non-unity SWR. Almost all auto-tuner algorithms seek minimum SWR. However, we no longer believe that minimum SWR is the best goal for a tuner placed at the antenna. The algorithm should seek a particular complex reflection coefficient, and SWR is blind to reflection coefficient phase. A radio amateur stands to gain a significant fraction of a dB increase in EIRP, a significant amount to serious contesters.

Acknowledgments

The author wishes to thank Dan Maguire, AC6LA, Larry Bos, WØPSI, and Luitjens Popken for correspondence and discussion that led to the writing of this paper. The author is indebted to Dean Straw, N6BV, for Example 1 and to Dan Maguire for the other examples. Dan and Larry independently did numerical comparison and confirmation of the formulas shown in **Table 3**. The graphs in **Figures 1 – 3** are Dan's (see **[17]**); the rest are the author's.

Steve Stearns, K6OIK, started in ham radio while in high school at the height of the Heathkit era. He holds an Amateur Extra class license and a commercial General Radio Operator license with radar endorsement. He previously held Novice, Technician, and First Class Radiotelephone licenses. He studied electrical engineering at California State University Fullerton, the University of Southern California, and Stanford, specializing in electromagnetics, communication engineering and signal processing. Steve was a Technical Fellow of Northrop Grumman Corporation before retirement. He worked at the Northrop Grumman Electromagnetic Systems Laboratory in San Jose, California, where he led the development of advanced communication signal processing systems, circuits, antennas, and electromagnetic devices. Steve is vice-president of the Foothills Amateur Radio Society, and served previously as Assistant Director of ARRL Pacific Division. He has authored more than 80 professional publications and ten patents. Steve has received numerous awards for professional and community volunteer activities.

References

[1] S. D. Stearns, K6OIK, "General Uniform Transmission Lines: Power Efficiency, Loss, Standing Wave Ratio, and Return Loss," *QEX*, no. 320, pp. 12-23, May/June 2020. Errata p. 6, Sep./Oct. 2020.

[2] C. G. Montgomery, R.H. Dicke, and E.M. Purcell, *Principles of Microwave Circuits*, MIT Rad. Lab. Series Volume 8, McGraw-Hill, 1948. Page 147.

[3] R. E. Colin, *Foundations for Microwave Engineering*, McGraw-Hill, 1966; 2nd Ed., McGraw-Hill, 1992, reissued by IEEE/Wiley, 2001, pp. 268-276, Eq. 4.87.

[4] D. C. Youla, "On Scattering Matrices Normalized to Complex Port Numbers," *Proc IRE*, vol. 49, no. 7, p. 1221, July 1961.

[5] K. Kurokawa, "Power Waves and the Scattering Matrix," *IEEE Trans. Microwave Theory and Techniques*, vol. 13, no. 2, pp. 194-202, Mar. 1965.

[6] C. Michaels, W7XC, "Complex Transmission Line Characteristic Impedance — How Important Is It?" *QST*, vol. 81, no. 11, pp. 70-71, Nov. 1997.

[7] R. H. Johnston and M. Okoniewski, "Propagation of New Power Waves On a Complex Impedance Transmission Line," *IEEE Int. Symp. Antennas and Propagation*, Fajardo, Puerto Rico, June 26-July 1, 2016.

[8] R. H. Johnston, "New Power Wave Network Analyses and Power Reciprocity," *IEEE Canadian Conference on Electrical and Computer Engineering*, Edmonton, Alberta, Canada, May 5-8, 2019.

[9] R. King, "Transmission-Line Theory and Its Applications," *J. Applied Physics*, vol. 14, no. 11, pp. 577-600, Nov. 1943; errata, vol. 15, no. 3, p. 292, Mar. 1944.

[10] R. W. P. King, *Transmission Line Theory*, McGraw-Hill, 1955; Dover 1965.

[11] A. E. Kennelly, *The Application of Hyperbolic Functions to Electrical Engineering Problems*, McGraw-Hill and Univ. London Press, 1912.

[12] W. W. Macalpine, "Computation of Impedance and Efficiency of Transmission Line with High Standing-Wave Ratio," *Trans. AIEE*, vol. 72, no. 3, pp. 334-339, July 1953.

[13] H. P. Westman, editor, *Reference Data for Radio Engineers*, 4th Ed., ITT, 1956. Pages 564-566.

[14] W. M. Middleton, editor, *Reference Data for Engineers: Radio, Electronics, Computers, and Communications*, 9th Ed., Newnes/Butterworth-Heinemann, 2002. Pages 29-10 to 29-12.

[15] R. D. Straw, N6BV, "*TLW* (Transmission Line for Windows): Version 3.24," Feb. 7, 2014, **www.arrl.org/files/file/QST%20Binaries/June2014/TLW3.zip**.

[16] S. D. Stearns, K6OIK, "A Transmission Line Power Paradox and Its Resolution," *ARRL Pacificon Antenna Seminar*, Oct. 10, 2014, **www.fars.k6ya.org/docs/k6oik**.

[17] D. Maguire, AC6LA, "Additional Loss Due to SWR is in Quotes for a Reason," **https://www.ac6la.com/swrloss.html**.

Luiz Duarte Lopes, CT1EOJ

Rua do Vale, 13A, Rinchoa, 2635-342 Rio de Mouro, Portugal; **ct1eoj@gmail.com**

Designing an Impedance Matching Network with a Drafting Ruler and Triangle

Solve a matching network graphically using drafting implements – no computer needed.

Nowadays we are very dependent on computers. Radio amateurs are no exception, both when operating digital modes, and also in the design and evaluation of antennas or electronic circuits where computers are a valuable tool.

But are we enslaved by computers and cannot take a step without their intervention? To show that we can do something without the aid of a computer, I used drafting tools to solve a problem that radio amateurs often face. It is the connection of a transmitter to an antenna through an impedance matching network. We will use a graduated ruler, a 45°/90° square, a drawing compass and a very sharp pencil, see **Figure 1**.

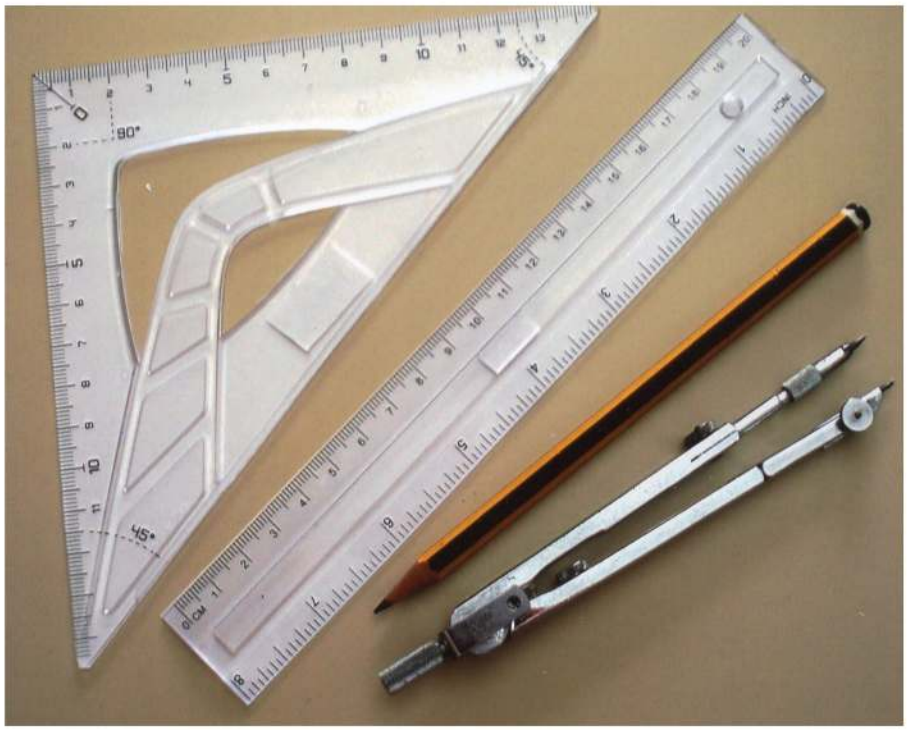

Figure 1 — Drawing tools.

Our Problem

As our example we will consider the L matching network shown in **Figure 2**. The antenna is a relatively short vertical on 14.215 MHz, with impedance, $Z_a = R_a - jX_a = (15 - j45)\ \Omega$. The radiation resistance is characteristically low and the reactance negative as is typical of a short antenna. It is fed with 50 Ω coaxial transmission line.

We begin with some simple calculations. Assuming 100 W output power of our transmitter, we easily determine the current I_0 at the input of the matching network and the current I_a at the output,

$$I_0 = \sqrt{\frac{100}{50}} = 1.414 \text{ A}$$

and

$$I_a = \sqrt{\frac{100}{15}} = 2.582 \text{ A}.$$

Voltage V_0 is at the network input and V_a is at the network output. V_a is the vector sum of V_{RA} and V_{XA} ,which are the voltages developed by current I_a respectively in the radiation resistance R_a and in the reactance X_a of the antenna.

$$V_0 = I_0 Z_0 = 1.414 \times 50 = 70.71 \text{ V}$$
$$V_{RA} = I_{ra} Z_{ra} = 2.582 \times 15 = 38.73 \text{ V}$$
$$V_{XA} = I_{xa} Z_{xa} = 2.582 \times 45 = 116.19 \text{ V}.$$

The Drawing

Now we move on to the drawing. We are going to represent voltages and currents with vectors having certain lengths in millimeters, so we need to define the respective scales. I used 10 mm for 10 V and 25 mm for 1 A on my sketch sheet.

We start our drawing (**Figure 3**) by defining on the sheet of paper a point **A**, from which the entire vector diagram will be developed according to the following steps. Note that since it is practically impossible to draw straight line segments with accuracy better than 0.5 mm, all values are rounded in the drawing to the nearest 0.5 mm. Use a very sharp pencil!

Step 1 – Plot the vector **AB** corresponding to the antenna input current I_a = 2.582 A (64.55 mm on my scale).

Step 2 – In-phase with the previous vector, mark the vector **AC** corresponding to the voltage that the current in the antenna develops in the radiation resistance, V_{RA} = 38.73 V (38.73 mm).

Step 3 – From point **C**, trace the vector **CD** (116.19 mm) perpendicular to the vector **AB**. This new vector corresponds to the voltage V_{XA} (116.19 V) developed in the reactive component of the antenna impedance by the current I_a. This reactive component of the antenna is negative, so V_{XA} has a phase delay of 90° relative to I_a.

Step 4 – Join point **A** with point **D**, to obtain the vector sum of the two previous vectors (122.5 mm) with the value of 122.5 V. This is the voltage V_a at the input terminals of the antenna and, simultaneously, at the terminals of capacitor *C*.

Step 5 – From point **B**, draw a line perpendicular to the vector **AD**. Simultaneously with a drawing compass centered on **A** and the opening of 35.35 mm corresponding to the input current I_0 = 1.414 A, make the intersection with this line at point **E**. Two vectors result in **AE** corresponding to the input current into the network, and another vector **BE** (91 mm), corresponding to the current flowing into the capacitor (I_C = 3.62 A).

Step 6 – Since the input voltage V_0 (vector **AF**) is in-phase with current I_0, in the extension of **AE** we can now mark the point **F**, corresponding to the voltage V_0 (70.71 mm).

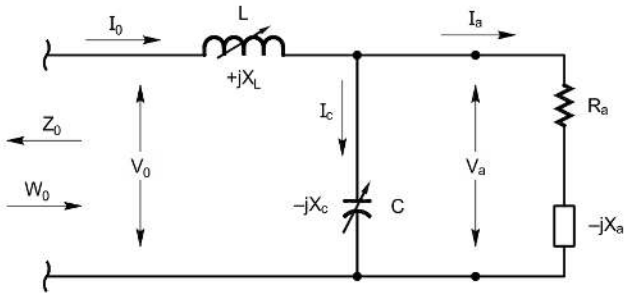

Figure 2 — An L-matching network.

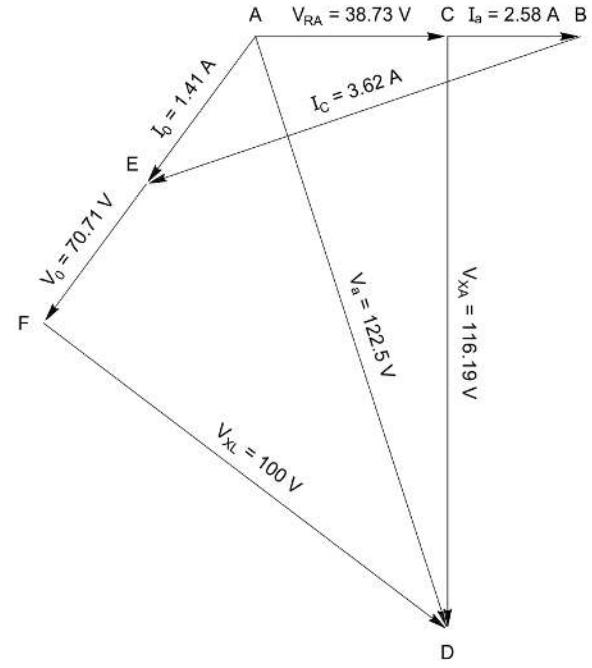

Figure 3 — Vector diagram graphical solution.

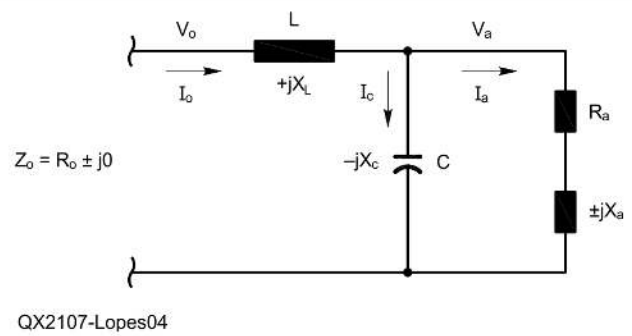

Figure 4 — Circuit for the Excel solution, where f is 14.215 MHz, R_a is 15 Ω, X_a is –45 Ω, and R_0 is 50 Ω. The resulting L and C are listed in Table 1.

Step 7 – Finally, join point **F** with point **D** to obtain a vector of 100 mm corresponding to the voltage V_{XL} = 100 V at the terminals of coil *L*. If the work has been done with reasonable care, this **FD** vector must be perpendicular to the voltage vector **AF**, given that in the coil *L* the current has a phase delay of 90° relative to the voltage at its terminals.

Final Calculations

Once we know all the current and voltage values, we can now return to our small calculator to obtain the value of the two reactances X_L and X_C.

$$X_L = V_{XL} / I_0 = 100 / 1.414 = 70.72$$

$$X_C = V_a / I_C = 122.5 / 3.62 = 33.84 .$$

Now, with the working frequency *f* in MHz, the following values are obtained for *L* and *C*:

$$L = \frac{X_L}{2\pi f} = \frac{70.72}{2\pi \times 14.215} = 0.79\ \mu\text{H}$$

$$C = \frac{10^6}{2\pi f X_C} = \frac{10^6}{2\pi \times 14.215 \times 33.84} = 330.85\ \text{pF} .$$

For another working frequency, a new vector diagram must be drawn, since the antenna impedance is certainly different.

Confirmation

To confirm the accuracy of our exercise, I entered the same data into an *Excel* spread sheet that I had written earlier. The *Excel* solution was based on the circuit of **Figure 4**. The results obtained, shown in **Table 1**, confirm the validity of this graphic method.

Table 1 – Confirming the validity of the graphical result.

L or C	*Drawing*	*Excel*	*Error*
L	0.79 µH	0.79 µH	0.00
C	330.85 pF	329.48 pF	1.37 pF (<0.5%)

I hope you enjoyed doing this exercise. Try another case with different data and different cells. By the way, do not throw away your computer.

Luiz Lopes, CT1EOJ, is an electrotechnical engineer who graduated from Porto University in Portugal in 1953. Luiz joined the Civil Aviation of Portugal as a telecommunications engineer for airports and air navigation services. There, he dealt with HF/VHF air-ground communications, HF point-to-point communications and the radio aids for air navigation. He retired as Director General for Air Navigation Services after 40 years of service. Luiz was first licensed in 1993.

Maynard A. Wright, W6PAP

6930 Enright Dr., Citrus Heights, CA 95621; **m-wright@eskimo.com**

SWR Dependence on Amplifier Output Impedance

SWR measurements by a bridge inline with a transmitter are affected by the output impedance of the transmitter.

In "Thoughts on Amplifier Output Impedance," **[1]** we showed that the output impedance of an RF amplifier need not be the same as the impedance of the line or other equipment that the amplifier is feeding. Will this affect the accuracy of equipment that measures various quantities at the output of the amplifier? Let's think about that a bit.

We'll consider SWR measurements made by a bridge circuit that separates the incident wave from the reflected wave and displays the values of each and/or calculates the reflection coefficient and/or SWR from those measurements. Bridges intended for this purpose today generally use inductive coupling to measure the current in the path through the instrument **[2]** and are often called directional wattmeters or SWR bridges depending on how they are configured and exactly what they measure and display. Complete suppression of the signal in the unwanted direction depends on an accurate ratio between voltage across the line and current in the line for that signal. This depends, in turn, on the impedance presented by the circuit that terminates the port of the bridge into which the signal is flowing **[3]**.

We'll be using *Spice Opus* **[4]** to model the bridge. To avoid complications with modeling RF transformers in *Spice Opus*, we'll use the Micromatch circuit **[5]**, that uses a series resistor in the path to sample the current flow rather than inductive coupling.

We'll model the circuit as in **Figure 1**, where the small numbers represent *Spice* nodes. The bridge uses 1 Ω in series with the line through the unit as does the similar SWR bridge shown in Figure 44 on page 457 of **[6]**. We've split the resistor into two 0.5 Ω resistors, R1 and R2, so we can measure the incident signal and the reflected signal simultaneously.

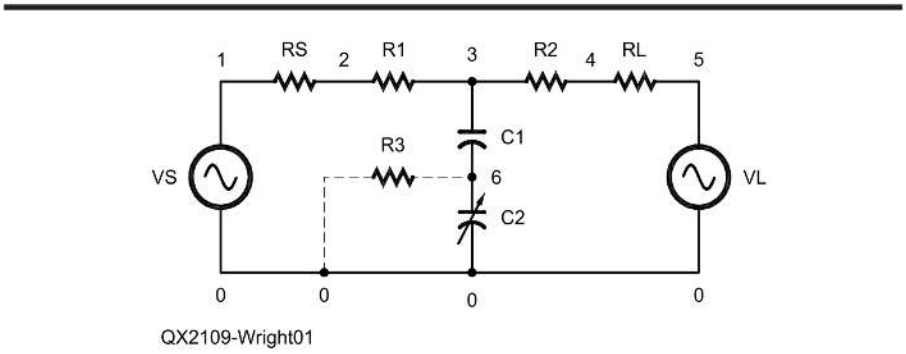

Figure 1 — SWR bridge circuit with source and load.

VS and RS represent the transmitter, and VL and RL represent the reflected voltage and impedance of the matching circuit or transmission line connected to the "antenna" side of the Micromatch. The *Spice Opus* script that analyzes this circuit is listed in **Table 1**. We'll tell *Spice Opus* to calculate and display the voltage between Nodes 2 and 6 (incident signal) and Nodes 4 and 6 (reflected signal), which is what additional physical circuitry in the Micromatch would do if we were to build one.

Resistor R3 is not a part of the bridge circuit, but is required to provide a dc ground path to Node 6. *Spice* requires such a dc path to ground for all nodes. Since R3 is not a part of the bridge, but is simply a high value resistor intended to make *Spice Opus* happy, it's drawn in **Figure 1** in dotted format. R3 is high enough in value to pass a negligible current and to therefore have essentially no effect on the operation of the bridge. Values of the components are:

VS = 2 V or 0 V
RS = 50 Ω or as described in the text
VR = 2 V or 0 V
RL = 50 Ω or as described in the text
R1 = 0.5 Ω
R2 = 0.5 Ω
R3 = 1e20 MΩ

The remaining components are C1 and C2. We chose those to cause approximately 0.2 mA to flow from Node 3 to ground (Node 0) when the frequency is 3.5 MHz and the voltage at Node 2 is 1.0 V. We could

calculate values for C1 and C2 by writing and solving simultaneous equations for each of the two current loops in **Figure 1**. It's easier, though, to think of the components on the right side of the circuit as a bridge **[7]** that we would like to be balanced when VR, the reflected signal voltage, is zero. We can achieve that by setting:

XC1 / XC2 = R2 / RL

We get the following capacitor values for 0.2 mA at 3.5 MHz:

C1 = 918.55 pF

C2 = 9.1855 pF

At frequencies other than 3.5 MHz, the current through the capacitors will differ from 0.2 mA, but the voltage division will remain the same and the bridge will function correctly in our model for all frequencies. C2 is shown as adjustable as it probably would be in an actual implementation.

So let's try the bridge to see how it works. We first set both RS and RL to 50 Ω. We set VS to 2.0 V **[8]** and VL to 0 V. We measure the magnitude of the voltage between nodes 6 and 2 using **[9, 10]**:

Vfwd = abs(v(6) – v(2))

This represents the voltage due to the forward traveling wave with any reflected wave balanced out by the bridge. We'll measure the voltage between Nodes 6 and 4 using:

Vref = abs(v(6) – v(4))

where Vref denotes the voltage associated with the reflected wave. Vref would ideally be zero when VR is zero, but it will consist, in the following calculations, of a residual value due to the presence of R3 in the circuit.

We use these values to calculate the SWR using **[11]**:

swr = (Vfwd + Vref) / (Vfwd – Vref) (1)

For 50 Ω on both sides, we get **[12]**:

vfwd = 1.980198e–02

vref = 1.113606e–16

swr = 1.000000e+00

Now let's change RS and RL to 70 Ω each and run the *Spice Opus* code again:

vfwd = 1.699306e–02

vref = 2.808722e–03

swr = 1.396031e+00

Note that the imbalance between the voltages at Node 2 (current measurement) and Node 6 (voltage measurement) is upset considerably by the change in impedance away from the design value. We'll change the two impedances to 35.7 Ω each:

vfwd = 2.371320e–02

vref = 3.911139e–03

swr = 1.395023e+00

For transmission lines of 70 and 35.7 Ω characteristic impedance, our bridge gives us an SWR indication that differs from 1.0 even when there is no reflected signal present. Rounding each of these results to SWR = 1.4 gives us agreement with exactly what Bird specifies that its Type 43 directional wattmeter **[13]** will see if it is inserted in circuits that present each of these impedances to both sides of the wattmeter and in which there is no reflected signal present. In the case of our *Spice Opus* circuit, and in the Bird directional wattmeter, the departure from SWR = 1.0 is due to unbalance of the bridge circuit caused by terminating the bridge in other than the design impedance. Our essentially exact agreement with Bird should give us confidence in our model.

So what will happen if we insert our SWR bridge between our hypothetical amplifier described in **[1]** and a 50 Ω load? The output impedance of our amplifier turned out to be 17.928 + j31.434 Ω as calculated by moving the source voltage to the output side of the amplifier. We can change RS to this complex impedance by changing the *Spice Opus* specification of RS to:

RS 1 9 17.928

LS 9 2 1.4289uH

where we chose Node 9 to be beyond the range of the other nodes just to flag us that it is temporary. The two lines are listed in **Table 1** but commented out. When we use this impedance on the "transmitter" side of the SWR bridge, we get:

vfwd = 2.647574e–02

vref = 3.330669e–16

swr = 1.000000e+00

Note that we changed only the impedance of the transmitter and left the load at 50 Ω. If we were to adjust the antenna tuner or prune the antenna to present 50 Ω resistive to the SWR bridge, it appears that the SWR would be 1.0 regardless the output impedance of the transmitter.

A little experimentation shows that the SWR indicated by voltage measurements in our bridge indicates the SWR that would be caused by a mismatch between a 50 Ω transmitter and the impedance of the load, rather than between the actual transmitter and the same load. This results from the fact that the bridge's ratio of sampled voltage to sampled current was chosen for a 50 Ω circuit. This is not bad in most cases, because the results may be closer to what the user anticipates than would be a calculation of the SWR based on the impedance of the transmitter and the impedance of the load.

If, for instance, we leave RS set to the output impedance from **[1]** and change RL to, first, 70 Ω and then 35.7 Ω, we find that we'll get the same results that we did when we change both RS and RL to each of those values while the source impedance RS was 50 Ω.

The results above all assume that there is no reflected signal returning from the line. The transmission line that returns reflected power back toward the transmitter must be represented by both VL and RL, with the actual values, which may be complex rather than real as in our simplified circuit, being determined by the ratio between the incident voltage and reflected voltage, including their phase angles with respect to each other. We won't delve deeply into that here, but will simply demonstrate that when there is reflected voltage present on the output side of the SWR bridge, the indicated SWR will be dependent on the output impedance of the transmitter as well as the magnitude of the returning signal.

We begin by leaving RS and RL in **Table 1** at 50 Ω each and changing VL to 0.5 V. We get the following output upon running the code:

vfwd = 1.980198e–02

vref = 4.950495e–03

swr = 1.666667

We can verify this by calculating the SWR using **Eqn (1)**.

Next we change the source impedance in **Table 1** to the output impedance of our hypothetical transmitter from **[1]**, by un-commenting the commented out RS and LS in **Table 1** and by commenting out the

Table 1 – Spice Opus script that analyzes the circuit of Figure 1.

```
VS 1 0 DC 0 AC 2
VL 5 0 DC 0 AC 0
RS 1 2 50
* RS 1 9 17.928
* LS 9 2 1.4289uH
R1 2 3 0.5
R2 3 4 0.5
RL 4 5 50
C1 3 6 918.55pF
C2 6 0 9.1855pF
R3 6 0 1e20Meg
* outputs
.control
ac lin 1 3.50MEGHz 3.50MEGHz
Vfwd = abs(v(6) - v(2))
Vref = abs(v(6) - v(4))
SWR = (Vfwd + Vref) / (Vfwd - Vref)
print Vfwd
print Vref
print SWR
.endc
.end
```

RS that is set to 50 Ω. When we execute the code, we get:

vfwd = 2.447208e–02
vref = 4.95095e–03
swr = 1.507182

Note that the measured SWR has dropped by about 11% from the value that we would expect. That's not very much, but the important point here is that the measured SWR when there is a reflected signal present is dependent on the output impedance of the transmitter.

We could calculate the error in SWR due to output impedance for various values of impedance, but to graph SWR versus real and reactive components in the source impedance would require a three dimensional graph or a family of two dimensional curves and the result might not be useful enough to justify the effort.

Conclusions

1 – The measurement of SWR by a bridge inline with a transmitter will be affected by the output impedance of the transmitter.

2 – It may not be possible to approach as closely as you would like to an SWR of 1.0 when you are using an inline bridge and your transmitter or transceiver to make a measurement.

3 – For SWR values near 1.0, the effect will be minor.

4 – The best match (minimum returned signal) will still be indicated by the lowest SWR measurement.

5 – Differences between measurements from inline SWR bridges or directional wattmeters and antenna analyzers may be due to the effects discussed here.

Maynard Wright, W6PAP, was first licensed in 1957 as WN6PAP. He holds an FCC General Radiotelephone Operator's License with Ship Radar Endorsement and is a Registered Professional Electrical Engineer in California. Maynard was involved in the telecommunications industry for over 48 years and is now retired. He has served as technical editor in several telecommunications standards and holds several patents. He is an ARRL member, A life Senior Member of IEEE, a Past Chairman of the Sacramento Section of ICCC, and a life Member and Past President of the North Hills Radio Club in Sacramento, California.

References

[1] M. Wright, W6PAP, "Thoughts on Amplifier Output Impedance," *QEX*, May/Jun.,2021, pp. 19-23.

[2] *The ARRL Handbook for Radio Communications 2020, Vol. 6*, Figure 25.59, p. 25.39.

[3] L. G. McCoy, W1ICP, "The Monimatch," *QST*, Oct., 1956, pp. 11-14.

[4] *Spice Opus* version 2.25 Light; **www.spiceopus.com**, this is an older 32-bit version of *Spice Opus* that is still available for download for use with 32-bit OS, Kubuntu 18.04.1 in this case.

[5] W. B. Bruene, WØTTK, "An Inside Picture of Directional Wattmeters," *QST*, Apr., 1959, Figure 3, p. 25.

[6] W. I. Orr, W6SAI, Editor, *The Radio Handbook*, Fifteenth Edition, 1959.

[7] *The ARRL Handbook for Radio Communications*, Vol. 6, Chapter 25, Figure 25.2: although intended for dc in this reference, a bridge configuration such as the Wheatstone bridge can also be useful in ac circuit applications.

[8] I generally use 2.0 V as a source voltage because when impedances are matched, the voltage at the junction between the source and the load will be 1.0 V.

[9] We let *Spice Opus* calculate to its full precision and retain the significant figures that are produced by the code. That's significant when dealing with differences among numbers that vary over several orders of magnitude.

[10] The article on the Micromatch adds the voltages across the resistor and capacitor in the circuit because the voltages are specified with respect to the junction between the two circuit elements. It's convenient in *Spice Opus* to specify voltages with respect to ground (Node 0) and we are accordingly subtracting the voltages between Nodes 2 and 6 (incident wave) and between Nodes 4 and 6 (reflected wave), rather than adding them. That's equivalent mathematically to the specification of addition in the article.

[11] *Reference Data for Radio Engineers, Fourth Edition*, International Telephone and Telegraph Corporation, 1956, p. 563.

[12] Although we are capitalizing variable names such as "SWR" in the text, the Output from *Spice Opus* is lower case and we've listed it that way here.

[13] *Bird RF Directional Thruline® Wattmeter Model 43 Operation Manual*, Instruction Book Part Number 920-43, Rev. L, Bird Technologies, Inc. 2016, p. 13.

Eric P. Nichols, KL7AJ

AlasKit Educational and Scientific Resources, 3763 Lyle Ave., North Pole, AK 99705; **kl7aj72@gmail.com**

Self-Paced Essays — #7 More KCL and KVL

Essay 7: Organize your analysis by writing down everything you know about each and every component in the circuit.

In our previous essay, we introduced two of the "biggies" in electrical engineering: Kirchhoff's Voltage Law (KVL), and Kirchhoff's Current Law (KCL). In this essay we will explore an interesting and informative circuit using a combination of both laws.

Let's first establish a couple of good practices that, while perhaps being a bit tedious at first, will greatly reduce confusion later on. When encountering a complex circuit, before performing any analysis, *write down everything you know* about each and every component in the circuit. It helps to write all these values *right next* to each component in question on your schematic. This might not always be easy. Sometimes finding a component value is the end product of the problem in the first place. But most of the time, we can quickly determine a few things about each component upon inspection. I call this practice of identifying every known value as *NSTATMI* (No Such Thing As Too Much Information). One distinct advantage of *NSTATMI* is that it almost always suggests several different ways of solving the problem.

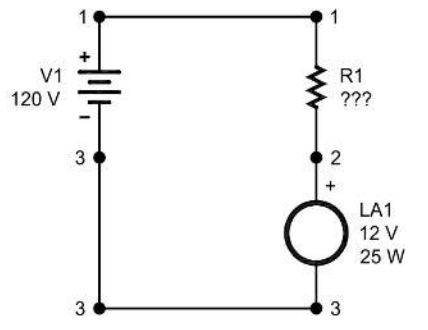

Figure 1 — A simple series circuit.

For a dc circuit, each and every component will have, as a bare minimum, a voltage drop value, a current value, a resistance value, and a power dissipation value. Keep in mind that *zero* is a perfectly valid number, as is *infinity*! Again, we might not be able to determine all of these values upon inspection, but if you *can*, then do so!

Consider the circuit of **Figure 1**. We have a simple series circuit, consisting of a 120 V voltage source V1, an unknown resistor R1 and a 12 V 25 W incandescent lamp LA1.

Our task is to find out what value of resistance R1 will result in the lamp LA1 operating at its rated voltage, 12 V.

Let's begin by learning everything there is to know about LA1. We know the voltage drop; it's specified as 12 V. This is non-negotiable. We know the power dissipation; it's 25 W, also non-negotiable. Do we know the resistance of the lamp? Not yet. And finally, do we know the current through the lamp? Not yet.

Now let's set up some tables of all the information we have about all our components. This may seem a bit overkill, but later on we will be using *matrices* to work out all kinds of complex problems, so it won't hurt to get used to the idea here. I call these prototypical matrices the *NSTATMI* tables. We start with **Table 1**.

Note that V1 is a *source,* so it generates power, which must equal all the power dissipated everywhere else in the circuit.

There's no particular order in which these have to be considered, however, it's usually helpful to start with the component having the least number of unknowns. So let's investigate LA1 first. We know the power dissipation and the voltage drop across LA1. What other value can we determine with the least amount of effort? How about current? We know by the power formula, $P = IE$ that we can figure out the current I by simply dividing the power by the voltage E. So that gives us 25/12 = 2.083 A. Remember the value, 2.083; we will need that later.

Do we know the resistance of LA1? Not yet. But we do know that a form of Ohm's Law, $R = E/I$, gives us 12/2.083 = 5.76 Ω. Now we can fill out the entire (**Table 2**) entry for LA1.

Next we consider R1. Initially we knew absolutely nothing about R1, but by virtue of Kirchhoff's Current Law (KCL), we can determine the current. We have three nodes in the circuit, 1, 2, and 3. Each of these nodes has exactly two *ports*, an input port and an output port. KCL tells us that the current entering each node has to equal the current leaving each node, so by extension, we have to have the same value of current *anywhere* in the circuit. This is extremely handy. So we know

Table 1 – The initial *NSTAMI* table.

Label	*Resistance*	*V drop*	*Current*	*Power*
LA1	Unknown	12 V	Unknown	25 W (dissipated)
R1	Unknown	Unknown	Unknown	Unknown
V1	0 Ω	120 V	Unknown	Unknown (sourced)

the current through R1 *must* be 2.083 A.

What about the voltage drop across R1? Well, remember the "red before black" method of measuring series voltage drops in the previous essay? If we apply that here, we have +120 V across the battery, a negative voltage across R1, and a negative 12 V across LA1. According to Kirchhoff's *voltage* law, (KVL) all these voltages have to add up to zero. So our negative voltage across R1 must be a −108 V. A resistor doesn't really care about the polarity of the voltage applied, so we can call the voltage across R1 simply 108 V. KVL to the rescue!

How about the resistance of R1? Once again we revert to Ohm's Law to get R1 = 108/2.083 = 51.85 Ω since the current *I* is the same everywhere in the circuit. We could actually stop here, because we now have the final answer, but we'll continue on, in order to fill out our tables, which will allow us to double-check all our work.

We also know the power dissipated in R1, which is found by $P = IE = 2.083 \times 108 = 225.0$ W. Obviously, this is not the most efficient circuit to satisfy the LA1 parameters, but it works. Let's fill out the entire **Table 3** row for R1.

Last, we fill out the rest of the chart for the V1 row. From KCL the current must be 2.083 A, just like everywhere else in the circuit. And the *power generated* by the source is calculated by $P = IE = 2.083 \times 120 = 250.0$ W

Now, we perform a sanity check. The power sourced by V1 should equal the total power dissipated by R1 and LA1. 250 W does indeed equal 225 W + 25 W, and we can fill in the entire **Table 4** for all values.

Now we can appreciate the utility of these handy little tables?

We end with a homework assignment. Show *two* additional methods, using the generated tables, to calculate the power dissipated by R1, the total circuit resistance, and the internal resistance of LA1 [Note that the *cold filament* resistance of an incandescent lamp, as measured with an ohm meter, will differ by an order of magnitude from its the operating (*hot filament*) resistance shown in **Table 4**. — *Ed.*]. As always, show all your work and send your answers to **kl7aj72@gmail.com**.

One final note. In this example, we assumed that V1 has no internal resistance. What happens if V1 has some internal resistance? That will be the topic of the entire upcoming essay on the Maximum Power Transfer theorem.

Until next time, stay safe and keep those soldering irons hot. (Yes you can do both simultaneously!) — *73, Eric Nichols. KL7AJ.*

Table 2 – LA1 row now known.

Label	*Resistance*	*V drop*	*Current*	*Power*
LA1	5.76 Ω	12 V	2.083 A	25 W (dissipated)
R1	Unknown	Unknown	Unknown	Unknown
V1	0 Ω	120 V	Unknown	Unknown (sourced)

Table 3 – R1 row now known.

Label	*Resistance*	*V drop*	*Current*	*Power*
LA1	5.76 Ω	12 V	2.083 A	25 W (dissipated)
R1	51.85 Ω	108 V	2.083 A	225 W (dissipated)
V1	0 Ω	120 V	Unknown	Unknown (sourced)

Table 4 – All values known.

Label	*Resistance*	*V drop*	*Current*	*Power*
LA1	5.76 Ω	12 V	2.083 A	25 W (dissipated)
R1	51.85 Ω	108 V	2.083 A	225 W (dissipated)
V1	0 Ω	120 V	2.083 A	250 W (sourced)

Upcoming Conferences

Digital Communications Conference (DCC)

September 17 – 19, 2021

Virtual

https://tapr.org/digital-communications-conference-dcc/

The 40th annual ARRL and TAPR Digital Communications Conference (DCC) will take place, September 17 – 19, 2021. Due to the coronavirus pandemic, this year's conference will be held online.

Technical papers are being solicited for presentation. Papers will also be published in the *Conference Proceedings*. Authors do not need to participate in the conference to have their papers included in the *Proceedings*. The submission deadline is **August 15, 2021**. Submit papers via email to Maty Weinberg, KB1EIB, **maty@arrl.org**. Papers will be published exactly as submitted, and authors will retain all rights.

Paper and presentation topic areas include, but are not limited to, software defined radio (SDR), digital voice, digital satellite communication, digital signal processing (DSP), HF digital modes, adapting IEEE 802.11 systems for amateur radio, Global Positioning System (GPS), Automatic Position Reporting System (APRS), Linux in amateur radio, AX.25 updates, Internet operability with Amateur Radio networks, TCP/IP networking over amateur radio, mesh and peer-to-peer wireless networking, emergency and homeland defense backup digital communications in amateur radio.

39th Annual Space Symposium

October 29 – 30, 2021

Bloomington, Minnesota

https://www.amsat.org/39th-annual-amsat-space-symposium-and-annual-general-meeting/

AMSAT-NA has issued its first call for papers for the 39th Annual AMSAT Space Symposium, set for October 29 – 31, 2021, at the Crowne Plaza AiRE hotel in Bloomington, Minnesota. Proposals for symposium presentations are invited on any topic of interest to the amateur satellite community. A tentative presentation title is requested, with final copy submitted by October 18 for inclusion in the symposium Proceedings. Send abstracts and papers to Dan Schultz, N8FGV, **n8fgv@amsat.org**.

Build Your Go-Kit with DX Engineering!

DX ENGINEERING

Coaxial Cable Assemblies

These low-loss cable assemblies are available in standard lengths with DX Engineering's revolutionary patented PL-259 connector. Use the online Custom Cable Builder at DXEngineering.com to build assemblies made to your exact specs. DX Engineering's coaxial cable is also available by the foot or in bulk spools. **Enter "DXE Cable" at DXEngineering.com.**

iPortable NANUK GATOR Cases

Equipment Cases

Protect your sensitive equipment! DX Engineering boasts three rugged options to keep your gear safe: virtually indestructible Gator Equipment Rack Cases for transporting everything you need in your Go-Kit; high-impact resin NANUK cases, including units that perfectly fit RigExpert Antenna Analyzers; and iPortable units that combine a travel case with a DC power distribution point, speaker, and rack shelving. **Enter "Equipment Case" at DXEngineering.com.**

DC Outlet Panels and Battery Backup Systems

West Mountain RADIO

Bid farewell to that annoying tangle of spaghetti wire with RIGrunner DC outlet panels from West Mountain Radio. These outlets are fused for protection and ensure you have reliable power distribution. They provide 40 amps of maximum power and include from 4 to 12 Powerpole® connectors. West Mountain also makes backup devices, such as the Super PWRgate, which instantly switches to battery backup if you lose power. **Enter "West Mountain" at DXEngineering.com.**

ASTRON CORPORATION YAESU AMERITRON KENWOOD ALINCO samlexamerica

Power Supplies

Make DX Engineering your source for reliable switching and linear power supplies from major brands, including Alinco, Ameritron, Astron, Samlex, Yaesu, and more. Choose from units with input voltages from 85 to 260 Vac and peak outputs from 10 to 50 amps. **Enter "Power Supplies" at DXEngineering.com.**

Antenna Tuners

DX Engineering carries a great lineup of LDG Electronics innovative automatic tuners to match just about any antenna and maximum power handling requirement, from 100 to 1,000 watts. Select from the 100W IT-100 model, which is ideal for Icom rigs; the 100W YT-100, designed for specific Yaesu radios; the QRP-friendly Z-817 auto-tuner; and the new Z-100A that can be interfaced with dozens of modern transceivers. **Enter "LDG Tuner" at DXEngineering.com.**

LDG ELECTRONICS

DX ENGINEERING

Portable Antennas

Need a versatile and easy-to-transport antenna? You'll find it here! Models include DX Engineering's EZ-BUILD UWA Center T and End Insulator Kits that let you build virtually any wire antenna type; Icom's 40-10M Magnetic Loop Antenna for the IC-705; a wide selection of rugged Comet HT and mobile antennas for upgraded performance; options from Chameleon, including the F-Loop Portable, EMCOMM II and III HF antennas, and HF Backpack Antenna Systems; AlexLoop's HamPack Portable Magnetic Loop Antenna System; and many more. **Enter "Portable Antenna" at DXEngineering.com.**

IC-705 HF/50/144/430 Portable Transceiver

ICOM

With the features and functionality of the IC-7300, IC-7610, and IC-9700, Icom's new QRP rig is like owning a base transceiver you can hold in one hand. It boasts SDR Direct Sampling technology for stellar transmit and receive performance; 4.3" color touchscreen; real-time spectrum scope and waterfall display; built-in Bluetooth®; wireless LAN; and full D-STAR capabilities. IC-705 accessories include backpack (ICO-LC-192) and compact automatic tuner (ICO-AH-705). **Enter "IC-705" at DXEngineering.com.**

ON ALL BANDS

DX Engineering's Amateur Radio Blog for New and Experienced Hams.
Visit OnAllBands.com for information you can use to improve your on-air experience.

YAESU ICOM KENWOOD ALINCO RM ITALY PRYME HEIL SOUND GENERAC

Request Your New Catalog Today at DXEngineering.com!

DX ENGINEERING®

Ordering (via phone) Country Code: +1
9 am to midnight ET, Monday-Friday
9 am to 5 pm ET, Weekends

Phone or e-mail Tech Support: 330-572-3200
9 am to 7 pm ET, Monday-Friday
9 am to 5 pm ET, Saturday

Ohio Curbside Pickup:
9 am to 8 pm ET, Monday-Saturday
9 am to 7 pm ET, Sunday

Nevada Curbside Pickup:
9 am to 7 pm PT, Monday-Sunday

800-777-0703 | DXEngineering.com

ON ALL BANDS YouTube

We're All Elmers Here! Ask us at: Elmer@DXEngineering.com
Email Support 24/7/365 at DXEngineering@DXEngineering.com

THE BRAINS OF THE OPERATION

BAR GRAPH
Visual representation of all gain and front-to-rear of all antennas

MAXIMUM GAIN MODE
Optimized for max gain

MAXIMUM FRONT-TO-REAR MODE
Optimized for best front to rear

3/4 MODE
Turns the BigIR vertical into a 3/4 wave antenna on 21-54 MHz

BEAM WIDTH
Lets you know the beam-width of chosen antenna designs

OptimizIR

The OptimizIR electronic controller is available as an upgrade for all SteppIR antenna products or as a standalone purchase.

AUTOTRAK
Antenna follows your radio wherever you tune for an optimized experience on every frequency

CUSTOM ANTENNA MODELS
Upload your models to controller

BI-DIRECTIONAL MODE
Simultaneous gain in opposite directions

180 MODE
Reverse directions at the click of a button

ELEMENT RETRACT MODE
Retract element during extreme weather events

steppIR COMMUNICATION SYSTEMS

FOR PRODUCT DETAILS AND ORDERING:
www.steppir.com 425-453-1910